https://erjm.journals.ekb.eg
ISSN: 1110-1180

DOI: ---------

ERJ
Engineering Research Journal
Faculty of Engineering
Menoufia University

Effect of Heat Transfer and Slipping on MHD peristaltic Flow with Suspended Particles

Muhammad M. Ahmed*, Ahmed G. Nasr, Ramzy M. Abumandour

Basic Engineering Sciences Department, Faculty of Engineering, Menoufia University, Egypt.

**(Corresponding author: : eng.mohamed928@yahoo.com)*

Abstract

This paper undertakes a comprehensive examination to theoretically assess the impact of magnetohydrodynamics (MHD), heat transfer, wall slip effects, and wall roughness on peristaltic flow incorporating suspended particles within an inclined channel immersed in porous media. The primary objective of this research is to afford a precise comprehension of fluid dynamics, specifically the peristaltic flow of vital fluids such as blood and their constituents within the human circulatory system. Furthermore, the implications of these findings extend to both biological and industrial domains magnetic resonance imaging (MRI) and radiosurgery applications. The governing equations encompassing continuity, momentum, and energy have been rigorously employed to model the intricate dynamics of the flow, with the perturbation method adroitly applied to analytically solve these inherently heterogeneous equations. The resultant analytical expressions, elucidating the interdependence of current, temperature, and pressure gradient, constitute pivotal outcomes of this investigation. Critical to the study is a meticulous analysis, inclusive of the visualization of the impact of various physical factors on key flow properties, such as the streamline function and axial velocity function. The software (Mathematica) is utilized for plotting the diverse effects on speed and pressure gradient. It is noteworthy that an escalation in wall slip manifests as a proportionate increase in the axial velocity of the fluid. Additionally, it is observed that the augmentation of the magnetic field correlates with an increase in the pressure difference, a trend that diminishes with higher degrees of wall slip. Furthermore, an enhancement in the permeability coefficient is found to positively influence both fluid velocity and particle velocity.

Keywords: *Magnetohydrodynamics (MHD),Porous media, Wall roughness , Peristaltic flow*

NOMENCLATURE

$\bar{X}, \bar{Y}$	Cartesian coordinate	t	dimensionless time
$\bar{U}, \bar{V}$	velocity components	Nr	thermal radiation parameter
S	drag force between the particle and fluid	u, v	dimensionless component of velocity
c_w	wave propagation velocity	Pr	Prandtl number
$\bar{t}$	Time	Gr	Grashof number
a	wave amplitude	M	Hartmann number
λ	wave wavelength	θ	dimensionless temperature
d	half channel width	δ	wave number
a_1	wall roughness height	β	heat source / sink parameter
$\bar{q}_r$	heat flux	Re	Reynolds number
$\bar{T}$	temperature	N	suspension factor
β_0	constant heat addition/absorption	ρ_0	article loading
K	and thermal conductivity	ε_1	amplitude ratio of the wave
A	molecules mean free path	ε_2	amplitude ratio of the wall roughness
α	coefficient of linear thermal expansion	λ'	wall roughness pitch ratio
λ_1	wall roughness pitch	F	dimensionless volume flow rate
$\acute{\varepsilon}$	mean Absorption Coefficient	p	dimensionless pressure
K'	Stefan- Boltzmann constant	ψ	dimensionless stream function
C	particles' constant volume fraction	Kn	Knudsen number
$\bar{p}$	pressure	k_0	permeability of the fluid
μ	liquid viscosity	ρ	density
ϕ	inclines of the channel on a horizontal axis	k_p	Permeability parameter of the porous area
σ	fluid electrical conductivity	Subscripts	
B_0	magnetic field strength	f	fluid
g	acceleration of gravity	p	particles

Introduction

In recent decades, there has been a notable surge in research devoted to the analysis of peristaltic motion within channels or tubes, driven by its significant applications in the realms of biomedical, industrial, and bioengineering disciplines. It is imperative to comprehend the inherent characteristics of peristaltic motion, characterized by the generation of fluid transport waves along a flexible wall, thereby inducing regions of relaxation and contraction along the extensible tube or channel containing the fluid. Physiologists have increasingly acknowledged peristalsis as a pivotal transport mechanism in various biological systems, manifesting in essential physiological processes across diverse bodily organs. Peristaltic motion is observed in vital physiological functions such as food propulsion through the esophagus, the transport of digested food within the digestive tract, bile conveyance via the bile duct, urine transportation from the kidney to the bladder, particle movement within the respiratory system, the transit of spermatozoa through the ductus efferent in the male reproductive tract, ciliary and ovum displacement through the fallopian channel, lymphatic vessel-mediated lymph transport, embryo conveyance in the non-pregnant uterus, and the propulsion of blood through arteries, venules, and capillaries. In situations necessitating fluid transport sans internal moving components like pistons, peristaltic pumping emerges as a preferable solution. In the biomedical domain, peristaltic pumps serve critical functions as components of lung-heart machines and blood pumps, facilitating the maintenance of blood circulation and oxygenation during open-heart surgeries by cyclically withdrawing blood from vessels, re-oxygenating it, and propelling it through arteries without compromising blood cell integrity. Beyond the biomedical context, peristaltic pumps find extensive utility in industrial applications, including the petroleum sector for the extraction of crude oil from porous rock, the conveyance of sanitary and corrosive fluids, and the handling of hazardous fluids in industrial sectors such as oil production, paper manufacturing, and the food industry. Moreover, in the nuclear industry, peristaltic transport of deleterious liquids is employed to prevent environmental contamination. Motivated by the pioneering work of Latham [1], who employed analytical and experimental methodologies to investigate urine flow through the ureter, researchers have delved into theoretical and experimental explorations of peristaltic motion. Subsequent studies, such as those by Jaffrin and Shapiro [2] , elucidated the influence of Reynolds numbers on peristaltic transport in channels, while Barton and Raylor [3] examined peristaltic flow through tubes using long and short wavelength approximations. Fung and Yih [4] employed perturbation techniques to analyze peristaltic free pumping at moderate amplitudes, revealing critical pressure gradients resulting in zero velocities on the channel centerline. Additionally, Mishra and Rao [5] investigated the peristaltic flow of Newtonian viscous fluids through asymmetric channels, elucidating enhancements in reflux and trapping zones within symmetric channels based on their research findings.

Magnetohydrodynamics (MHD) pertains to the investigation of the influence exerted by a magnetic field on the dynamics of diverse fluid media. In recent decades, this field has garnered considerable attention due to the abundance, significance, and versatility of its applications in both medical and industrial domains [6]. Notably, the utilization of MHD flow under peristalsis has been observed in various medical applications, encompassing drug targeting, casting processes, magnetic blood pumping, mitigation of surgical bleeding, magnetotherapy, pulsed therapy for tibial fractures, osteoporosis treatments, spinal lumbar fusion [7], rotary maglev cardiac-assist devices, and the pumping of biological and chemical samples, including DNA and saline buffers. Sud et al. [8] conducted a study on the pumping effect of a magnetic field on blood, emphasizing its practical application. Their investigation revealed the feasibility of blood pumping through the application of a slowly moving axial magnetic field, requiring a modest number of magnets (108 amp turns/meter) to generate a robust and steady blood pumping current. Agrawal and Anwaruddin [9] delved into the impact of a magnetic field on blood flow through a uniformly branching channel, employing a foundational mathematical model for blood. Their findings suggested that the influence of a magnetic field could be harnessed as a blood pump during medical surgeries. Mekheimer [10]examined blood peristaltic flow in nonuniform tubes under the influence of a magnetic field, determining that an

increase in the magnetic field strength corresponds to a rise in maximum pressure. Mustapha et al. [11] explored the effects of a uniform transverse magnetic field on the flow of an electrically conducting fluid representing blood through irregularly shaped arteries.

Their investigation demonstrated that the flow separation area diminishes with increasing magnetic field strength, ultimately disappearing with a sufficiently high magnetic field intensity. Loukopoulos and Tzirtzilakis [12] investigated the impact of a uniform magnetic field on bio-magnetic (blood) fluid through a curved squared duct. Their findings highlighted the importance of considering blood's electrical conductivity in the presence of a uniform magnetic field. Tzirtzilakis and Xenos [13] studied the effects of a continuous localized magnetic field on bio-magnetic fluid in a driven cavity, revealing that the existence of a magnetic field significantly influences the flow. Sharma et al. [14] contributed to the discourse by examining hydro-magnetic non-Newtonian blood transport with an orthogonal magnetic field impacting the surface, inferring that the presence of a magnetic field holds considerable potential for practical applications in controlling blood circulation.

In the realm of industrial applications, the magnetic field emerges as a pivotal factor, exerting profound influence across diverse sectors. Notably, its significance extends to areas such as astrobiology, geothermal energy, Magnetohydrodynamics (MHD) generators, and aerospace engineering. Similarly, within the medical domain, the magnetic field plays a crucial role, finding extensive applications in Magnetic Resonance Imaging (MRI), medical technology, petroleum operations, and nuclear reactors. The investigation conducted by El-Shehawey et al. [15] delves into the impact of MHD on the peristaltic flow of viscoelastic fluids. Their findings reveal a noteworthy trend wherein an augmentation in the magnetic field correlates with a decrement in velocity. Subsequently, Hayat et al. [16] explore the influence of induced magnetic fields on the pressure gradient and stream function of an incompressible fluid exhibiting peristaltic motion, employing the long-wavelength method. The discerned outcome indicates a rise in pressure proportional to the magnetic field strength, while streamlining demonstrates a reduction in the size of the trapped bolus, eventually leading to its disappearance. Furthermore, Rashid et al. [17] contribute to the discourse by investigating the ramifications of an induced magnetic field within a curved channel on peristaltic flow for an incompressible Williamson fluid. Their discernments elucidate a pronounced increase in pressure specifically for the Williamson fluid in comparison to other viscous fluids. Abumandour et al.[18] present a theoretical framework elucidating the influence of magnetohydrodynamics (MHD) on viscous compressible flow in the presence of slip conditions. Their findings suggest that augmenting magnetic flux induces a resistance to the flow, resulting in a reduction of the mean axial streamwise velocity. Furthermore, the investigation reveals that elevated levels of magnetic flux contribute to the manifestation of reverse flow within the channel core. These observations underscore the intricate interplay between MHD effects and slip conditions in shaping the dynamics of compressible flows.

The investigation of peristaltic motion in fluid transport, prevalent in both physiological systems within the human body and various industrial applications, holds substantial significance. In numerous instances, the thermal conditions of the conveyed fluid diverge from the ambient environment, engendering heat transfer phenomena in accordance with thermodynamic principles. The comprehensive analysis of peristaltic flow under the influence of heat transfer emerges as a crucial endeavor, contributing to a nuanced understanding of these complex systems. Within the medical domain, heat transfer plays a pivotal role in diverse applications such as the assessment of cutaneous burns, exploration of oxygenation and hemodialysis mechanisms, targeted destruction of malignancies, investigation of blood flow through dilution techniques, and elucidation of heat flux arising from bloodstream dynamics, including membrane pores, radiation exchanges between bodily conditions and surfaces, vasodilation processes, and the intricacies of nourishment preparation. This academic discourse underscores the imperative nature of studying peristaltic flow in conjunction with heat transfer for the comprehensive comprehension of these multifaceted systems, particularly within the intricate landscape of medical applications.

In the realm of industrial applications, the heat transfer process assumes a pivotal role in diverse contexts such as the production of paper and the processing of food. Radhakrishnamacharya and Murty [19] conducted a comprehensive investigation into the nuanced impact of heat transfer on peristaltic motion within a non-uniform channel. Srinivas and Kothandapan [20], in their scholarly pursuit, delved into the intricate interplay between heat transfer and peristaltic flow of a viscous incompressible fluid traversing an asymmetrical channel. Their observations delineate that an augmented phase difference between the channel boundaries manifests as a diminishing temperature amplitude at the channel inlet. Nadeem and Akbar [21] contributed to the scholarly discourse by examining the ramifications of heat transfer on the peristaltic flow of magnetohydrodynamic (MHD) Newtonian fluid within an asymmetric channel, employing the Adomian decomposition method. Their discernments highlight a noteworthy augmentation in flow pressure concomitant with an escalation in the heat radiation factor. Mishra et al. [22], in their investigation, explored the influence of heat source and oscillatory suction on MHD, revealing that the presence of a heat source inhibits oscillatory flow, whereas a sink promotes it. Mahmood et al.[23] , utilizing the spectral homotropy analysis method, undertook a rigorous examination of the heat transfer impact of MHD fluid in divergent and convergent channels. Their principal findings underscore an enhancement in thermal profiles for elevated values of Reynolds and Nusselt numbers. Hayat et al. [24] undertook an analytical exploration into the effect of heat transfer on peristaltic MHD flow, concluding that, in comparison to hydrodynamic flow, MHD flow exhibits a heightened heat transfer coefficient. Qasim et al. [25] systematically investigated the impact of a magnetic field on entropy in two-dimensional peristaltic flow through numerical methods. Their results unequivocally demonstrate the analogous behavior of heat transfer under varying strengths of the magnetic field.

The presence of a porous medium is observed in physiological systems, notably in the modeling of arteries and respiratory mechanisms, where fatty deposits are prevalent. Additionally, porous media find relevance in various biological contexts such as the human lung, bile duct, and gall bladder with stones. Industrial applications also incorporate porous media in diverse fields, ranging from the extraction of crude oil from porous rock to sanitary fluid movement. Despite the significance of porous media in peristaltic mechanisms, prior research has not accorded them the due importance. El-Shehawey et al.[26] were pioneers in investigating the use of porous walls in peristaltic transport. Subsequently, El-Shehawey et al.[27] delved into the study of peristaltic flow in a cylindrical tube in the presence of a porous medium. The outcomes revealed that an increase in the permeability factor led to a rise in the mean axial velocity. Expanding on this, El-Shehawey et al.[28] explored the impact of porous media on peristaltic transport through a non-symmetric channel. Furthermore, the interplay of peristaltic transportation and magnetohydrodynamics within a porous space was investigated by Hayat et al.[29]. The thermal aspects of porous media were scrutinized by Umavathi et al.[30], emphasizing that a decrease in the permeability parameter corresponds to a reduction in temperature within both the porous and viscous fluid regions.

In numerous biological models, the influence of wall slipping parameters on flow properties has been a subject of considerable investigation. This phenomenon manifests across diverse applications, such as internal cavities and artificial heart valves. Chu and Fang [31] conducted an insightful examination into peristaltic transport under slipping conditions, establishing that the flow exhibits heightened instability in slip scenarios as compared to the conventional no-slip cases. Addressing the impact of a magnetic field, Ali et al. [32] elucidated the alterations in peristaltic fluid transport induced by slipping conditions. Notably, their findings underscored that an escalation in the slip parameter led to a discernible reduction in the diameter of trapped boluses. Sinha et al. [33] delved into the intricate interplay between wall slip and heat exchange, revealing that slip at the walls resulted in an augmentation of the mean streamwise velocity. Furthermore, Vajravelu et al. [34] conducted a comprehensive investigation into the combined effects of slipping, heat transfer, and concentration jump conditions on magnetohydrodynamic (MHD) peristaltic flow of a Carreau fluid through a non-uniform channel. Their study contributes to the nuanced understanding of the intricate dynamics governing fluid flow in such systems. Eldesoky et

al.[35] investigated the impact of slip conditions on the transport dynamics of particle-fluid within a catheterized pipe subjected to peristaltic motion. Employing perturbation techniques to solve the model, the researchers observed that the flow exhibited deceleration tendencies with escalating flow rates and amplitude ratios, irrespective of slip or nonslip conditions.

The investigation of particulate suspension has garnered significant attention from researchers owing to its extensive applications in both biological and industrial domains. In their seminal work, Hung and Thomas [36] conducted a thorough analysis of the motion exhibited by solid particles within two-dimensional peristaltic flows. Their model delineates the trajectory of a neutrally buoyant particle propelled along the channel's axis by a single bolus. Rath and Reese [37] delved into the peristaltic flow characteristics of non-Newtonian fluids containing particles, offering valuable insights relevant to industrial scenarios, particularly in the context of pumping non-Newtonian fluids with particulate content, such as in sanitary applications. Srivastava et al. [38] endeavored to elucidate the effects of Poiseuille flow on the peristaltic transport of particulate suspensions. In a parallel vein, Mekheimer et al. [39] explored peristaltic fluid flow with particle suspension through a planar channel, observing a reduction in the pumping rate with increasing particle density. Sara and Vafai [40], in their analysis of particulate suspension impact on peristaltically induced unsteady pulsatile flow within a narrow artery, discerned an expansion of the peristaltic region concurrent with an increase in particle concentration, coupled with a decrease in trapped bolus size. For compressible fluids, Eldesoky et al. [41] delved into the peristaltic transport of a compressible liquid containing suspended particles in a planar channel.

Subsequently, Eldesoky et al. [42] extended their investigation to encompass the combined thermal effects on peristaltically driven particle-fluid transportation through a porous channel. Their findings indicated a discernible decrease in temperature when fluid suspension was present. Expanding the scope to incorporate thermal radiation, slip conditions, and magnetohydrodynamics (MHD), Bhatti et al. [43] probed the impact on peristaltic pumping of dusty fluid through a porous medium duct. Their conclusive observation revealed that an augmentation in volume concentration led to a reduction in fluid velocity, as well as diminished fluid and particle temperatures. Kamel et al. [44] conducted an inquiry into the impact of slip phenomena on the peristaltic conveyance of a suspension comprising particles and fluid within a channel. The investigation employed perturbation techniques to address the mathematical model. The findings reveal that the critical reflux pressure is diminished in the presence of particle-fluid suspension as compared to particle-free fluid scenarios, indicating a discernible influence of slip conditions on this critical parameter.

Investigating the impact of wall roughness on fluid transport holds particular significance in comprehending diverse issues within both industrial and physiological domains. In physiological contexts, heightened roughness in arterial walls, resulting from the accumulation of fat, has been implicated in disrupting blood flow equilibrium, potentially culminating in clot formation [45], particularly within coronary arteries. This phenomenon underscores the criticality of understanding the implications of wall roughness in the biomedical sphere. In the industrial realm, the study of fluid transportation in the presence of walls demands attention to surface roughness, as nearly all surfaces exhibit some degree of irregularity. Undesirable consequences, such as impeding fluid movement and enhancing wall erosion, may arise in applications where wall roughness is a prominent characteristic. Conversely, in scenarios involving fluid mixing, augmenting wall roughness is often preferred to enhance the mixing process. Shukla et al. [46] conducted a comprehensive examination of surface roughness effects during peristaltic movement in a nonuniform channel. Their findings revealed a gradual increase in the roughness parameter corresponding to a proportional rise in maximum pressure. This observation was attributed to a concurrent reduction in the flow area, indicative of heightened surface roughness, thereby elevating the maximum pressure rise value. Subsequently, Shukla et al. extended their investigation into the influence of heat transfer during peristaltic transport through a rough nonuniform inclined channel[47]. The outcomes of this research bear relevance to the study of heat conduction within various bodily organs responsible for the transportation of biological fluids.

In light of the foregoing examination, it is apparent that the investigation into bio-fluid dynamics within channels characterized by wall roughness has been subject to limited scholarly scrutiny. Consequently, the principal objective of this study is to systematically elucidate the multifaceted influences of primary factors on biofluids, including magnetic fields, heat transfer, slip, and porous media, in the context of peristaltic propulsion. The focus is on a corrugated fluid laden with suspended particles within an inclined channel exhibiting wall roughness. The analytical framework adopted in this investigation employs a perturbation method to address the nonlinear equations inherent in this intricate phenomenon. This theoretical inquiry holds significant importance for attaining comprehensive insights into various physical phenomena associated with the peristaltic conveyance of biofluids within human physiological conduits. Moreover, the outcomes of this research carry substantial implications for a diverse array of industrial applications. The analysis rigorously explores the influence of diverse parameters on the profiles of streamlines, velocity, and pressure gradients. The discernment of the physical behavior of the considered parameters is explicated through meticulous graphical representation. The primary objective of this research is to provide a precise understanding of fluid dynamics, specifically focusing on the peristaltic flow of vital fluids, such as blood and their constituents, within the human circulatory system. Furthermore, the implications of these findings extend to both biological and industrial domains, including applications in magnetic resonance imaging (MRI) and radiosurgery.

Mathematical Formulation

Consider a Newtonian fluid in which a peristaltic wave facilitates the transportation of rigid particles through a uniformly inclined channel, characterized by a width of (2d). The channel incorporates a porous region, and its walls are maintained at consistent temperatures while being subjected to a magnetic field. The flow within the channel experiences the influence of both a temperature gradient and a heat source. It is essential to note that the channel walls exhibit sinusoidal-shaped wall roughness. The sinusoidal wave, characterized by a speed (c_w), propagates along the channel walls. The chosen Cartesian coordinate system positions the $\bar{X}$-axis parallel to the channel's longitudinal axis, aligning with the direction of the wave, while the $\bar{Y}$-axis remains normal to it. A graphical representation of the physical model is provided in Figure 1.

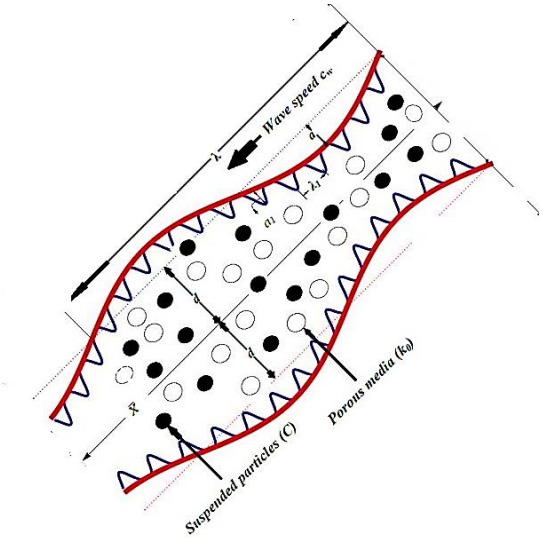

Figure1 Geometry of the problem

The geometries of the wall surfaces are given as in Shukla et al [46]

$$\text{upper wall } \bar{H}_1(\bar{X},\bar{t}) = d + a\sin\left(\frac{2\pi}{\lambda}(\bar{X} - c_w\,\bar{t})\right) - a_1\cos^4\left(\frac{\pi\bar{X}}{\lambda_1}\right) \quad (1)$$

$$\text{lower wall } \bar{H}_2(\bar{X},\bar{t}) = -d - a\sin\left(\frac{2\pi}{\lambda}(\bar{X} - c_w\,\bar{t})\right) + a_1\cos^4\left(\frac{\pi\bar{X}}{\lambda_1}\right) \quad (2)$$

The governing equations of continuity, linear momentum, and energy for fluid and particle phases in porous media with a magnetic field can be expresses as [49]-[51]:

Fluid-Phase

Continuity Equation

$$\frac{\partial}{\partial\bar{X}}[(1-C)\bar{U}_f] + \frac{\partial}{\partial\bar{Y}}[(1-C)\bar{V}_f] = 0 \quad (3)$$

Momentum equations

$$(1-C)\rho_f\left[\frac{\partial\bar{U}_f}{\partial\bar{t}} + \bar{U}_f\frac{\partial\bar{U}_f}{\partial\bar{X}} + \bar{V}_f\frac{\partial\bar{U}_f}{\partial\bar{Y}}\right] = -(1-C)\frac{\partial\bar{P}}{\partial\bar{X}} + (1-C)\mu\left(\frac{\partial^2\bar{U}_f}{\partial\bar{X}^2} + \frac{\partial^2\bar{U}_f}{\partial\bar{Y}^2}\right) + CS\left(\bar{U}_p - \bar{U}_f\right) + (1-C)\rho_f g\alpha_f(\bar{T} - T_0)\sin(\phi) - \sigma B_0^2\bar{U}_f - \frac{\mu}{k_0}U_f \quad (4)$$

$$(1-C)\rho_f\left[\frac{\partial \bar{V}_f}{\partial \bar{t}}+\bar{U}_f\frac{\partial \bar{V}_f}{\partial \bar{X}}+\bar{V}_f\frac{\partial \bar{V}_f}{\partial \bar{Y}}\right]=-(1-C)\frac{\partial \bar{P}}{\partial \bar{Y}}+$$
$$(1-C)\mu\left(\frac{\partial^2 \bar{V}_f}{\partial \bar{X}^2}+\frac{\partial^2 \bar{V}_f}{\partial \bar{Y}^2}\right)+CS\left(\bar{V}_p-\bar{V}_f\right)-\frac{\mu}{k_0}V_f \quad (5)$$

Energy equation

$$(1-C)\rho_f C_p\left[\frac{\partial \bar{T}}{\partial \bar{t}}+\bar{U}_f\frac{\partial \bar{T}}{\partial \bar{X}}+\bar{V}_f\frac{\partial \bar{T}}{\partial \bar{Y}}\right]=K\left[\frac{\partial^2 \bar{T}}{\partial \bar{X}^2}+\frac{\partial^2 \bar{T}}{\partial \bar{Y}^2}\right]+$$
$$\frac{\partial \bar{q}_r}{\partial \bar{Y}}+\beta_0 \quad (6)$$

Particulate-Phase:

Continuity Equation

$$\frac{\partial}{\partial \bar{X}}\left[C\,\bar{U}_p\right]+\frac{\partial}{\partial \bar{Y}}\left[C\,\bar{V}_p\right]=0 \quad (7)$$

The momentum equations

$$C\rho_p\left[\frac{\partial \bar{U}_p}{\partial \bar{t}}+\bar{U}_p\frac{\partial \bar{U}_p}{\partial \bar{X}}+\bar{V}_p\frac{\partial \bar{U}_p}{\partial \bar{Y}}\right]=-C\frac{\partial \bar{P}}{\partial \bar{X}}+C\,S\left(\bar{U}_f-\bar{U}_p\right)+C\rho_p g\alpha_p(\bar{T}-T_0)\sin(\phi) \quad (8)$$

$$C\,\rho_p\left[\frac{\partial \bar{V}_p}{\partial \bar{t}}+\bar{U}_p\frac{\partial \bar{V}_p}{\partial \bar{X}}+\bar{V}_p\frac{\partial \bar{V}_p}{\partial \bar{Y}}\right]=-C\frac{\partial \bar{P}}{\partial \bar{Y}}+CS\left(\bar{V}_f-\bar{V}_p\right) \quad (9)$$

With boundary conditions including wall slipping:

upper wall $\bar{U}_f-A\frac{\partial \bar{U}_f}{\partial \bar{Y}}=0 \quad ,\bar{T}=T_1$ at $\bar{Y}=\bar{H}_1(\bar{X},\bar{t})$ (10)

lower wall $\bar{U}_f+A\frac{\partial \bar{U}_f}{\partial \bar{Y}}=0 \quad ,\bar{T}=T_0$ at $\bar{Y}=\bar{H}_2(\bar{X},\bar{t})$ (11)

Overcome heat.

The heat flux ($\bar{q}_r$) can be expressed using Roseland approximation as:

$$\bar{q}_r=-\frac{4\,\acute{\varepsilon}}{3K'}\frac{\partial T^4}{\partial \bar{Y}} \quad (12)$$

Given that the temperature variance within the fluid mass that flows is sufficiently small, we can write by Taylor expansion and cancelling higher-order terms,

$$T^4\approx 4T_0^3\bar{T}-3T_0^4 \quad (13)$$

by substituting Equation. (13) into Equation. (12), we get,

$$\bar{q}_r=-\frac{16\,\acute{\varepsilon}\,T_0^3}{3K'}\frac{\partial T}{\partial \bar{Y}} \quad (14)$$

To simplify the peristaltic flow problem, it is convenient to describe the transformation of variables from the fixed frame$(\bar{X},\bar{Y},\bar{t})$ to the wave (laboratory) frame $(\bar{x},\bar{y})$

$$\bar{y}=\bar{Y}\ ,\bar{x}=\bar{X}-c_w\bar{t}\ ,\bar{u}_f=\bar{U}_f-c_w\ ,\bar{v}_f=\bar{V}_f,\bar{u}_p=\bar{U}_p-c_w\ ,\bar{v}_p=\bar{V}_p,T=\bar{T},\bar{p}(\bar{x},\bar{y})=\bar{P}(\bar{X},\bar{Y},\bar{t}). \quad (15)$$

By introducing non-dimensional quantities which can be used to simplify the moving boundary value problem:

$$y=\frac{\bar{y}}{d},x=\frac{\bar{x}}{\lambda},t=\frac{c_w\bar{t}}{\lambda},u_f=\frac{\bar{u}_f}{c_w},$$

$$u_p=\frac{\bar{u}_p}{c_w},v_f=\frac{\lambda\bar{v}_f}{d\,c_w},v_p=\frac{\lambda\bar{v}_p}{d\,c_w},$$

$$p=\frac{d^2\bar{p}}{c_w\lambda\mu},Nr=\frac{16\sigma' T_0^3}{3K'k},\theta=\frac{T-T_0}{T_1-T_0},$$

$$\delta=\frac{d}{\lambda},Kn=\frac{A}{d},Pr=\frac{\mu C_p}{K},$$

$$Gr=\frac{\rho g d^2\alpha(T_1-T_0)}{c\mu_0},M^2=\frac{\sigma d_1^2B_0^2}{\mu_0},k_p=\frac{k_0}{d^2},\beta=\frac{d^2\beta_0}{K(T_1-T_0)},\ Re=\frac{\rho_f dc_w}{\mu},\ N=\frac{S\,d^2}{(1-C)\mu},\rho_0=\frac{\rho_p}{\rho_f}. \quad (16)$$

. The geometry of the wall surfaces become.

upper wall $H_1(x,t)=1+\varepsilon_1\sin(2\pi x)-\varepsilon_2\cos^4\left(\frac{\pi(x+t)}{\lambda'}\right)$ (17)

lower wall $H_2(x,t)=-1-\varepsilon_1\sin(2\pi x)+\varepsilon_2\cos^4\left(\frac{\pi(x+t)}{\lambda'}\right)$ (18)

By applying Equation. (15) and Equation. (16) into Equation. (3) to Equation. (9) the Governing equations becomes:

Fluid-Phase

Continuity Equation

$$\frac{\partial}{\partial x}[(1-C)u_f]+\frac{\partial}{\partial y}[(1-C)v_f]=0 \quad (19)$$

The momentum equations

$$Re\,\delta\left[(u_f+1)\frac{\partial u_f}{\partial x}+v_f\frac{\partial u_f}{\partial y}\right]=-\frac{\partial p}{\partial x}+\left(\delta^2\frac{\partial^2 u_f}{\partial x^2}+\frac{\partial^2 u_f}{\partial y^2}\right)+CN\left(u_p-u_f\right)-\frac{M^2}{(1-C)}(u_f+1)+Gr\theta\sin(\phi) \quad (20)$$

$$Re\delta^3\left[(u_f+1)\frac{\partial v_f}{\partial x}+v_f\frac{\partial v_f}{\partial y}\right]=-\frac{\partial p}{\partial y}+\left(\delta^2\frac{\partial^2 v_f}{\partial x^2}+\frac{\partial^2 v_f}{\partial y^2}\right)+\delta CN\left(\bar{V}_p-\bar{V}_f\right) \quad (21)$$

The energy equation

$$(1-C)\mathrm{Re}\,\delta\,\mathrm{Pr}\left[(u_f+1)\frac{\partial\theta}{\partial x}+v_f\frac{\partial\theta}{\partial y}\right]=\delta^2\frac{\partial^2\theta}{\partial x^2}+\frac{\partial^2\theta}{\partial y^2}+N_r\frac{\partial^2\theta}{\partial y^2}+\beta \quad (22)$$

Particulate-Phase:

Continuity Equation

$$\frac{\partial}{\partial x}\left[C\,u_p\right]+\frac{\partial}{\partial y}\left[C\,v_p\right]=0 \quad (23)$$

The momentum equations

$$\mathrm{Re}\,\delta\,\rho_0\left[(u_p+1)\frac{\partial u_p}{\partial x}+v_p\frac{\partial u_p}{\partial y}\right]=-\frac{\partial p}{\partial \bar{X}}+CN(u_f-u_p)+\mathrm{Gr}\,\rho_0\sin(\phi) \quad (24)$$

$$\mathrm{Re}\,\delta^3\,\rho_0\left[(u_p+1)\frac{\partial v_p}{\partial x}+v_p\frac{\partial v_p}{\partial y}\right]=-\frac{\partial \bar{P}}{\partial \bar{Y}}+\delta CS(v_f-v_p) \quad (25)$$

For two-dimensional flow, the dimensionless stream function (ψ) expressed as

$$u=\frac{\partial\psi}{\partial y}\ ,\ v=-\frac{\partial\psi}{\partial x} \quad (26)$$

Applying Equation. (26) into Equation. (19) to Equation. (25) yields to:

Fluid-Phase

$$\frac{\partial^2\psi_f}{\partial x\,\partial y}-\frac{\partial^2\psi_f}{\partial x\,\partial y}=0 \quad (27)$$

$$\mathrm{Re}\,\delta\left[\left(\frac{\partial\psi_f}{\partial y}+1\right)\frac{\partial^2\psi_f}{\partial x\,\partial y}-\frac{\partial\psi_f}{\partial x}\frac{\partial^2\psi_f}{\partial y^2}\right]=-\frac{\partial p}{\partial x}+\delta^2\frac{\partial^3\psi_f}{\partial x^2\,\partial y}+\frac{\partial^3\psi_f}{\partial y^3}+\mathrm{Gr}\,\theta\sin(\phi)+CN\left(\frac{\partial\psi_p}{\partial y}-\frac{\partial\psi_f}{\partial y}\right)-\frac{M^2+\frac{1}{k_p}}{(1-C)}\left(\frac{\partial\psi_f}{\partial y}+1\right) \quad (28)$$

$$\mathrm{Re}\,\delta^3\left[-\left(\frac{\partial\psi_f}{\partial y}+1\right)\frac{\partial^2\psi_f}{\partial x^2}+\frac{\partial\psi_f}{\partial x}\frac{\partial^2\psi_f}{\partial y\,\partial x}\right]=-\frac{\partial p}{\partial y}-\delta^2\left(\delta^2\frac{\partial^3\psi_f}{\partial x^3}+\frac{\partial^3\psi_f}{\partial y^2\,\partial x}\right)-\delta^2 CN\left(\frac{\partial\psi_p}{\partial x}-\frac{\partial\psi_f}{\partial x}\right)+\frac{\delta^2}{(1-C)\,k_p}\left(\frac{\partial\psi_f}{\partial y}+1\right) \quad (29)$$

$$(1-C)\mathrm{Re}\,\delta\,\mathrm{Pr}\left[\left(\frac{\partial\psi_f}{\partial y}+1\right)\frac{\partial\theta}{\partial x}-\frac{\partial\psi_f}{\partial x}\frac{\partial\theta}{\partial y}\right]=\delta^2\frac{\partial^2\theta}{\partial x^2}+\frac{\partial^2\theta}{\partial y^2}+Nr\,\frac{\partial^2\theta}{\partial y^2}+\beta \quad (30)$$

Particulate-Phase:

$$\frac{\partial^2\psi_p}{\partial x\,\partial y}-\frac{\partial^2\psi_p}{\partial x\,\partial y}=0 \quad (31)$$

$$\mathrm{Re}\,\delta\,\rho_0\left[\left(\frac{\partial\psi_p}{\partial y}+1\right)\frac{\partial^2\psi_p}{\partial x\,\partial y}-\frac{\partial\psi_p}{\partial x}\frac{\partial^2\psi_p}{\partial y^2}\right]=-\frac{\partial p}{\partial x}+\rho_0\mathrm{Gr}\,\theta\sin(\phi)+(1-C)N\left(\frac{\partial\psi_f}{\partial y}-\frac{\partial\psi_p}{\partial y}\right) \quad (32)$$

$$\mathrm{Re}\,\delta^3\rho_0\left[-\left(\frac{\partial\psi_p}{\partial y}+1\right)\frac{\partial^2\psi_p}{\partial x^2}+\frac{\partial\psi_p}{\partial x}\frac{\partial^2\psi_p}{\partial y\,\partial x}\right]=-\frac{\partial p}{\partial y}-\delta^2(1-C)N\left(\frac{\partial\psi_f}{\partial x}-\frac{\partial\psi_p}{\partial x}\right) \quad (33)$$

Differentiating equation (28) with respect to (y) and equation (29) with respect to (x) then subtracting, the two equations we get:

$$\mathrm{Re}\,\delta\left[\left(\frac{\partial\psi_f}{\partial y}+1\right)\frac{\partial^3\psi_f}{\partial x\,\partial y^2}-\frac{\partial\psi_f}{\partial x}\frac{\partial^3\psi_f}{\partial y^3}\right]-\mathrm{Re}\,\delta^3\left[-\left(\frac{\partial\psi_f}{\partial y}+1\right)\frac{\partial^3\psi_f}{\partial x^3}+\frac{\partial\psi_f}{\partial x}\frac{\partial^3\psi_f}{\partial y\,\partial x^2}\right]=\delta^2\frac{\partial^4\psi_f}{\partial x^2\,\partial y^2}+\frac{\partial^4\psi_f}{\partial y^4}-\delta^2\left(\delta^2\frac{\partial^4\psi_f}{\partial x^4}+\frac{\partial^4\psi_f}{\partial y^2\,\partial x^2}\right)+\mathrm{Gr}\sin(\phi)\frac{\partial\theta}{\partial y}+CN\left(\frac{\partial^2\psi_p}{\partial y^2}-\frac{\partial^2\psi_f}{\partial y^2}\right)-\frac{M^2+\frac{1}{k_p}}{(1-C)}\frac{\partial^2\psi_f}{\partial y^2}-\delta^2 CN\left(\frac{\partial^2\psi_p}{\partial x^2}-\frac{\partial^2\psi_f}{\partial x^2}\right)+\frac{\delta^2}{(1-C)\,K_p}\frac{\partial^2\psi_f}{\partial y\,\partial x} \quad (34)$$

Differentiating equation (32) with respect to (y) and equation (33) with respect to (x) then subtracting, the two equations we get:

$$\rho_0\,\mathrm{Re}\,\delta\left[\left(\frac{\partial\psi_p}{\partial y}+1\right)\frac{\partial^3\psi_p}{\partial x\,\partial y^2}-\frac{\partial\psi_p}{\partial x}\frac{\partial^3\psi_p}{\partial y^3}\right]-\mathrm{Re}\,\delta^3\left[-\left(\frac{\partial\psi_p}{\partial y}+1\right)\frac{\partial^3\psi_p}{\partial x^3}+\frac{\partial\psi_p}{\partial x}\frac{\partial^3\psi_p}{\partial y\,\partial x^2}\right]=(1-C)N\left(\frac{\partial^2\psi_f}{\partial y^2}-\frac{\partial^2\psi_p}{\partial y^2}\right)-\delta^2 CN\left(\frac{\partial^2\psi_f}{\partial x^2}-\frac{\partial^2\psi_p}{\partial x^2}\right)+\rho_0\mathrm{Gr}\sin(\phi)\frac{\partial\theta}{\partial y} \quad (35)$$

Rate of Volume Flow

In the laboratory frame, the instantaneous volume flow rate is defined as

$$\overline{Q_f}=(1-C)\int_{\bar{H}_2(\bar{X},\bar{t})}^{\bar{H}_1(\bar{X},\bar{t})}\bar{U}_f(\bar{X},\bar{Y},\bar{t})\,d\bar{Y} \quad (36)$$

Similarly, the rate of volume flow in the wave frame is calculated as

$$\bar{q}=(1-C)\int_{\bar{H}_2(\bar{x},\bar{t})}^{\bar{H}_1(\bar{x},\bar{t})}\bar{u}_f(\bar{x},\bar{y})\,d\bar{y} \quad (37)$$

Using the conversions Equation. (15) in Equation. (36), and with Equation. (37), We obtain the following relationship between volumetric flow rates:

$$\overline{Q_f} = \bar{q} + c_w(\bar{H}_1(\bar{x},\bar{t}) - \bar{H}_2(\bar{x},\bar{t})) \quad (38)$$

The mean flow over a period T = $\left(\frac{\lambda}{c_w}\right)$ at a fixed position is defined as:

$$\widetilde{Q} = \frac{1}{T}\int_0^T \bar{Q}\, dt \quad (39)$$

By substituting (37) into (36) we get

$$\widetilde{Q} = \bar{q} + 2\, c_w\, d \quad (40)$$

Let (Q) be the dimensionless time mean flow, where.

$$F = \frac{\bar{q}}{c_w\, d}\ , Q_f = \frac{\bar{Q}_f}{c_w\, d} \quad (41)$$

We derive the next relations by using Equation. (39)

$$Q_f = F + 2 \quad (42)$$

The boundary conditions become:

upper wall $\psi_f = \frac{F}{2}$, $\frac{\partial \psi_f}{\partial y} - Kn\frac{\partial^2 \psi_f}{\partial y^2} = -1$,$\theta = 1$ at $y = H_1$ (43)

lower wall $\psi_f = -\frac{F}{2}$, $\frac{\partial \psi_f}{\partial y} + Kn\frac{\partial^2 \psi_f}{\partial y^2} = -1$,$\theta = 0$ at $y = H_2$ (44)

Solution Technique

The equation at hand is effectively addressed through the application of perturbation analysis methods. As elucidated in reference [48] ,this approach entails expressing the solution as the initial terms of an asymptotic expansion, typically limited to no more than two terms. These expansions are systematically conducted with respect to a parameter, either inherently present in the equation or artificially introduced for ease of analysis; such expansions are denoted as parameter perturbations. The efficacy of this methodology is underscored by its recurrent application in scholarly works, as evidenced by references [49]-[51]

Adhering to the tenets of perturbation analysis, the system of governing equations (19)-(35) is systematically tackled by employing parameter perturbation techniques for the variable (δ), within the confines of the specified boundary conditions (43) and (44). This leads to the derivation of zeroth and first-order systems of equations. Assuming the parameter (δ), a series expansion is then conducted for the pertinent properties, namely $u_{f,p}, v_{f,p}, \psi_{f,p}, \theta, p, F$, yielding expressions characterized by a discernible degree of precision and accuracy.

$$u = u_0 + \delta\, u_1 + \delta^2 u_2 + \cdots$$

$$v = v_0 + \delta\, v_1 + \delta^2 v_2 + \cdots$$

$$\psi = \psi_0 + \delta\, \psi_1 + \delta^2\, \psi_2 + \cdots$$

$$\theta = \theta_0 + \delta\, \theta_1 + \delta^2\, \theta_2 + \cdots \quad (45)$$

$$p = p_0 + \delta\, p_1 + \delta^2\, p_2 + \cdots$$

$$F = F_0 + \delta\, F_1 + \delta^2\, F_2 + \cdots$$

Zero order system:

$$0 = -\frac{\partial p_0}{\partial x} + \frac{\partial^3 \psi_{f0}}{\partial y^3} + Gr\sin(\phi)\,\theta_0 + C\,N\left(\frac{\partial \psi_{p_0}}{\partial y} - \frac{\partial \psi_{f_0}}{\partial y}\right) - z_1^2\left(\frac{\partial \psi_{f_0}}{\partial y} + 1\right) \quad (46)$$

$$0 = -\frac{\partial p_0}{\partial y} \quad (47)$$

$$\frac{\partial^2 \theta_0}{\partial y^2} = -\frac{\beta}{1+Nr} \quad (48)$$

$$0 = -\frac{\partial p_0}{\partial x} + \rho_0 Gr\sin(\phi)\ \theta_0 + (1-C)N\left(\frac{\partial \psi_{f_0}}{\partial y} - \frac{\partial \psi_{p_0}}{\partial y}\right) \quad (49)$$

$$\frac{\partial^4 \psi_{f_0}}{\partial y^4} - z_1^2\frac{\partial^2 \psi_{f_0}}{\partial y^2} = -\left[Gr\sin(\phi)\frac{\partial \theta_0}{\partial y} + CN\left(\frac{\partial^2 \psi_{p_0}}{\partial x^2} - \frac{\partial^2 \psi_{f_0}}{\partial x^2}\right)\right] \quad (50)$$

$$0 = (1-C)N\left(\frac{\partial^2 \psi_{f_0}}{\partial x^2} - \frac{\partial^2 \psi_{p_0}}{\partial x^2}\right) + \rho_0 Gr\sin(\phi)\frac{\partial \theta_0}{\partial y} \quad (51)$$

With Boundary conditions

upper wall $\psi_{f_0} = \frac{F_0}{2}$, $\frac{\partial \psi_{f_0}}{\partial y} - Kn\frac{\partial^2 \psi_{f_0}}{\partial y^2} = -1$,$\theta_0 = 1$ at $y = H_1$ (52)

lower wall $\psi_{f_0} = -\frac{F_0}{2}\frac{\partial \psi_{f_0}}{\partial y} + Kn\frac{\partial^2 \psi_{f_0}}{\partial y^2} = -1$,$\theta_0 = 0$ at $y = H_2$ (53)

The parameter z_1 is defined as $z_1^2 = \frac{M^2 + \frac{1}{k_p}}{(1-C)}$

The solution of zero order system:

$$\theta_0 = \frac{z_0}{2}y^2 + c_1 y + c_2 \quad (54)$$

$$\psi_{f0} = c_3\, e^{z_1 y} + c_4 e^{-z_1 y} + C_5 y + C_6 - \frac{z_3}{2\, z_1^2} y^2 - \frac{z_2}{6\, z_1^2} y^3 \quad (55)$$

$$\psi_{p0} = \frac{n_6}{z_1}\, e^{z_1 y} - \frac{n_7}{z_1} e^{-z_1 y} + \frac{n_8}{3} y + C_6 + \frac{n_9}{2} y^2 + n_{10} y + \frac{n_7}{z_1} - \frac{n_6}{z_1} \quad (56)$$

$$\frac{\partial p_0}{\partial x} = \rho_0 Gr \sin(\phi)\ \theta_0 + (1 - C) N \left(\frac{\partial \psi_{f_0}}{\partial y} - \frac{\partial \psi_{p_0}}{\partial y}\right) \quad (57)$$

First order system:

$$\mathrm{Re}\left[\frac{\partial \psi_{f_0}}{\partial y}\frac{\partial^2 \psi_{f_0}}{\partial x\, \partial y} + \frac{\partial^2 \psi_{f_0}}{\partial x\, \partial y} - \frac{\partial \psi_{f_0}}{\partial x}\frac{\partial^2 \psi_{f_0}}{\partial y^2}\right] = -\frac{\partial p_1}{\partial x} + \frac{\partial^3 \psi_{f_1}}{\partial y^3} + Gr \sin(\phi)\, \theta_1 + C N \left(\frac{\partial \psi_{p_1}}{\partial y} - \frac{\partial \psi_{f_1}}{\partial y}\right) - z_1^2 \frac{\partial \psi_{f_1}}{\partial y} \quad (58)$$

$$0 = -\frac{\partial p_1}{\partial y} \quad (59)$$

$$\frac{\partial^2 \theta_0}{\partial y^2} = \frac{1}{1+Nr}\left((1 - C)\, Pr\ Re\ \left[\frac{\partial \psi_{f_0}}{\partial y}\frac{\partial \theta_0}{\partial x} + \frac{\partial \theta_0}{\partial x} - \frac{\partial \psi_{f_0}}{\partial x}\frac{\partial \theta_0}{\partial y}\right]\right) \quad (60)$$

$$\mathrm{Re}\, \rho_0 \left[\frac{\partial \psi_{p_0}}{\partial y}\frac{\partial^2 \psi_{p_0}}{\partial x\, \partial y} + \frac{\partial^2 \psi_{p_0}}{\partial x\, \partial y} - \frac{\partial \psi_{p_0}}{\partial x}\frac{\partial^2 \psi_{p_0}}{\partial y^2}\right] = -\frac{\partial p_1}{\partial x} + \rho_0 Gr \sin(\phi)\ \theta_1 + (1 - C) N \left(\frac{\partial \psi_{f_1}}{\partial y} - \frac{\partial \psi_{p_1}}{\partial y}\right) \quad (61)$$

$$\frac{\partial^4 \psi_{f_1}}{\partial y^4} - z_1^2 \frac{\partial^2 \psi_{f_1}}{\partial y^2} = \mathrm{Re}\left[\frac{\partial \psi_{f_0}}{\partial y}\frac{\partial^3 \psi_{f_0}}{\partial x\, \partial y^3} + \frac{\partial^3 \psi_{f_0}}{\partial x\, \partial y^2} - \frac{\partial \psi_{f_0}}{\partial x}\frac{\partial^3 \psi_{f_0}}{\partial y^3}\right] - \left[Gr \sin(\phi)\frac{\partial \theta_1}{\partial y} + CN\left(\frac{\partial^2 \psi_p}{\partial x^2} - \frac{\partial^2 \psi_f}{\partial x^2}\right)\right] \quad (62)$$

$$\mathrm{Re}\, \rho_0 \left[\frac{\partial \psi_{p_0}}{\partial y}\frac{\partial^3 \psi_{p_0}}{\partial x\, \partial y^2} + \frac{\partial^3 \psi_{p_0}}{\partial x\, \partial y^2} - \frac{\partial \psi_{p_0}}{\partial x}\frac{\partial^3 \psi_{p_0}}{\partial y^3}\right] = (1 - C) N \left(\frac{\partial^2 \psi_{f_1}}{\partial x^2} - \frac{\partial^2 \psi_{p_1}}{\partial x^2}\right) + \rho_0 Gr \sin(\phi)\frac{\partial \theta_1}{\partial y} \quad (63)$$

With Boundary conditions

upper wall $\psi_{f_1} = \frac{F_1}{2}$, $\frac{\partial \psi_{f_1}}{\partial y} - Kn \frac{\partial^2 \psi_{f_1}}{\partial y^2} = 0$, $\theta_1 = 0$ at $y = H_1$ (64)

lower wall $\psi_{f_1} = -\frac{F_1}{2}$, $\frac{\partial \psi_{f_1}}{\partial y} + Kn \frac{\partial^2 \psi_{f_1}}{\partial y^2} = 0$, $\theta_1 = 0$ at $y = H_2$ (65)

The solution of first order system:

$$\theta_1 = I_1 \left(\frac{-2 + z_1 y}{z_1^3}\right) e^{z_1 y} + I_2 \left(\frac{2 + z_1 y}{z_1^3}\right) e^{-z_1 y} + \frac{I_3}{z_1^2}\, e^{z_1 y} + \frac{I_4}{z_1^2} e^{-z_1 y} + \frac{I_5}{20}\, y^5 + \frac{I_6}{12}\, y^4 + \frac{I_7}{6} y^3 + \frac{I_8}{2}\, y^2 + c_7\, y + c_8 \quad (66)$$

$$\psi_{f_1} = T_1 e^{2 z_1 y} + T_2\, e^{-2 z_1 y} + T_3\, y^3\, e^{z_1 y} + T_4\, y^3\, e^{-z_1 y} + T_5\, y^2\, e^{z_1 y} + T_6\, y^2\, e^{-z_1 y} + T_7\, y\, e^{z_1 y} + T_8\, y\, e^{-z_1 y} + T_9\, e^{z_1 y} + T_{10}\, e^{-z_1 y} + T_{11}\, y^6 + T_{12}\, y^5 + T_{13} y^4 + T_{14} y^3 + T_{15}\, y^2 + c_9\, e^{z_1 y} + c_{10}\, e^{-z_1 y} + c_{11}\, y + c_{12} \quad (67)$$

$$\psi_{p_1} = \frac{1}{60 N {Z_1}^4}\Big(30 e^{2yZ_1} {L_1 {Z_1}^3} - 30 e^{-2yZ_1} {L_2 {Z_1}^3} + y\big(60 L_{16} + y(30 L_{15} + 20 L_{14} y + 15 L_{13} y^2 + 12 L_{12} y^3 + 10 L_{11} y^4)\big) {Z_1}^4 + 60 e^{yZ_1}\Big(L_3\big(-6 + 6yZ_1 - 3y^2 {Z_1}^2 + y^3 {Z_1}^3\big) + Z_1\Big(Z_1(-L_7 + L_9 Z_1 + L_7 y Z_1) + L_5\big(2 - 2yZ_1 + y^2 {Z_1}^2\big)\Big)\Big) - 60 e^{-yZ_1}\Big(L_4\big(6 + 6yZ_1 + 3y^2 {Z_1}^2 + y^3 {Z_1}^3\big) + Z_1\Big(Z_1(L_8 + L_{10} Z_1 + L_8 y Z_1) + L_6\big(2 + 2yZ_1 + y^2 {Z_1}^2\big)\Big)\Big)\Big) + \frac{1}{2N {Z_1}^4}\big(-12(L_3 + L_4) + 4(L_5 - L_6) Z_1 - 2(L_7 + L_8) {Z_1}^2 + (L_1 - 2L_{10} - L_2 + 2L_9) {Z_1}^3\big); \quad (68)$$

$$\frac{\partial p_1}{\partial x} = -\mathrm{Re}\, \rho_0 \left[\frac{\partial \psi_{p_0}}{\partial y}\frac{\partial^2 \psi_{p_0}}{\partial x\, \partial y} + \frac{\partial^2 \psi_{p_0}}{\partial x\, \partial y} - \frac{\partial \psi_{p_0}}{\partial x}\frac{\partial^2 \psi_{p_0}}{\partial y^2}\right] + \rho_0 Gr \sin(\phi)\ \theta_1 + (1 - C) N \left(\frac{\partial \psi_{f_1}}{\partial y} - \frac{\partial \psi_{p_1}}{\partial y}\right) \quad (69)$$

$$\Delta p = \int_0^1 \frac{\partial p}{\partial x}\, dx \quad (70)$$

Graphical Results and Discussion

1.1 Validation Section

Validating the outcomes of our study necessitates a comprehensive comparison with antecedent investigations, and in this context, we turn our attention to the seminal work conducted by Elshehawey et al [28], who obtained results under analogous conditions. To conduct a meaningful comparison, certain parameters within our model were deliberately modified to align with the conditions

employed by Elshehawey and his colleagues. Specifically, we set the magnetic field (M) to zero, eliminated slipping effects (Kn = 0), nullified particle suspensions (C = 0), minimized wall roughness (ε_2 = 0), and eliminated the impact of heat transfer by setting the Grashof number (Gr) to zero. This meticulous adjustment was aimed at emulating the identical modeling conditions as Elshehawey.

Upon executing our modified model under these conditions and juxtaposing the results with those obtained by Elshehawey, as illustrated in Figure 2, a striking concordance between the outcomes is discernible. Despite the methodological divergence, wherein Elshehawey employed the Adomian decomposition method for solving the model, our results exhibit a notable similarity to those achieved by Elshehawey. This congruence strengthens the robustness and consistency of our findings, as they align closely with outcomes derived from an alternative mathematical approach. The congruence between our findings and those elucidated by Elshehawey serves to validate the resilience and universality inherent in our model. The deliberate replication of Elshehawey parameters not only accentuates the reproducibility of our results but also attests to the robustness of our approach across heterogeneous problem-solving methodologies. This sustained uniformity not only bolsters the credibility of our study but also underscores its scientific merit within the expansive landscape of academic discourse, thereby fortifying its contribution to the corpus of knowledge in the respective domain.

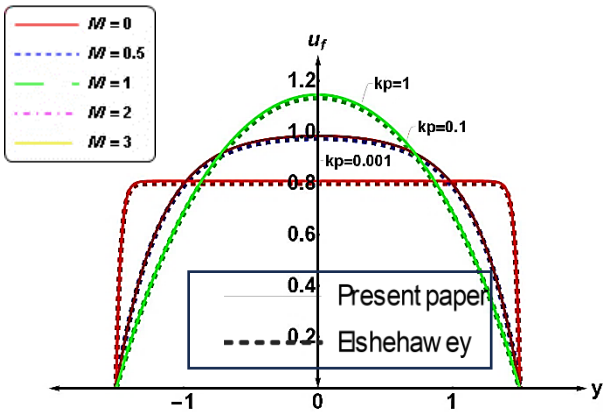

Figure 2 Influence of Permeability parameter (K_p) fluid flow behavior at at $\mathbf{\Delta p = 0; \varepsilon_1 = 0.7}$

1.2 Results and discussion

This section provides detailed elucidation of specific graphical outcomes pertaining to the influence of diverse parameters on both the fluid and particulate phases within a stenotic channel. The examination encompasses the effects of a magnetic field, slipping parameter, permeability parameter, Reynolds number, particle concentration, suspension factor, and wall roughness height ratio on the axial and total velocities of the fluid, as well as the axial and total velocities of particulate matter. Additionally, the investigation delves into the impact of these parameters on the pressure gradient and pressure difference within the system.

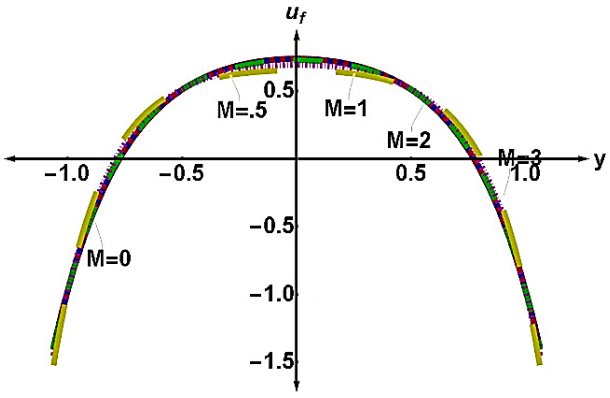

a)

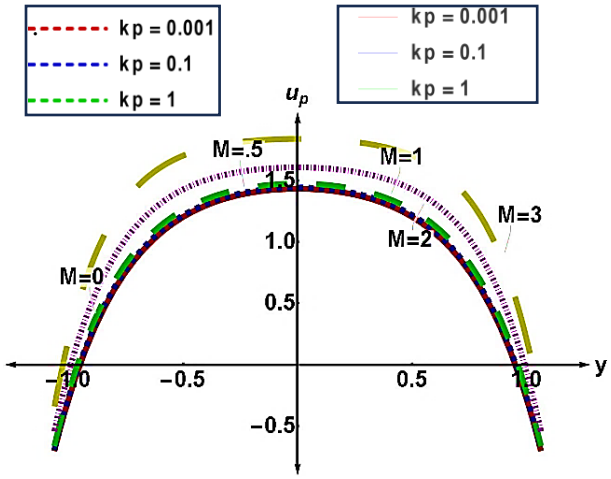

b)

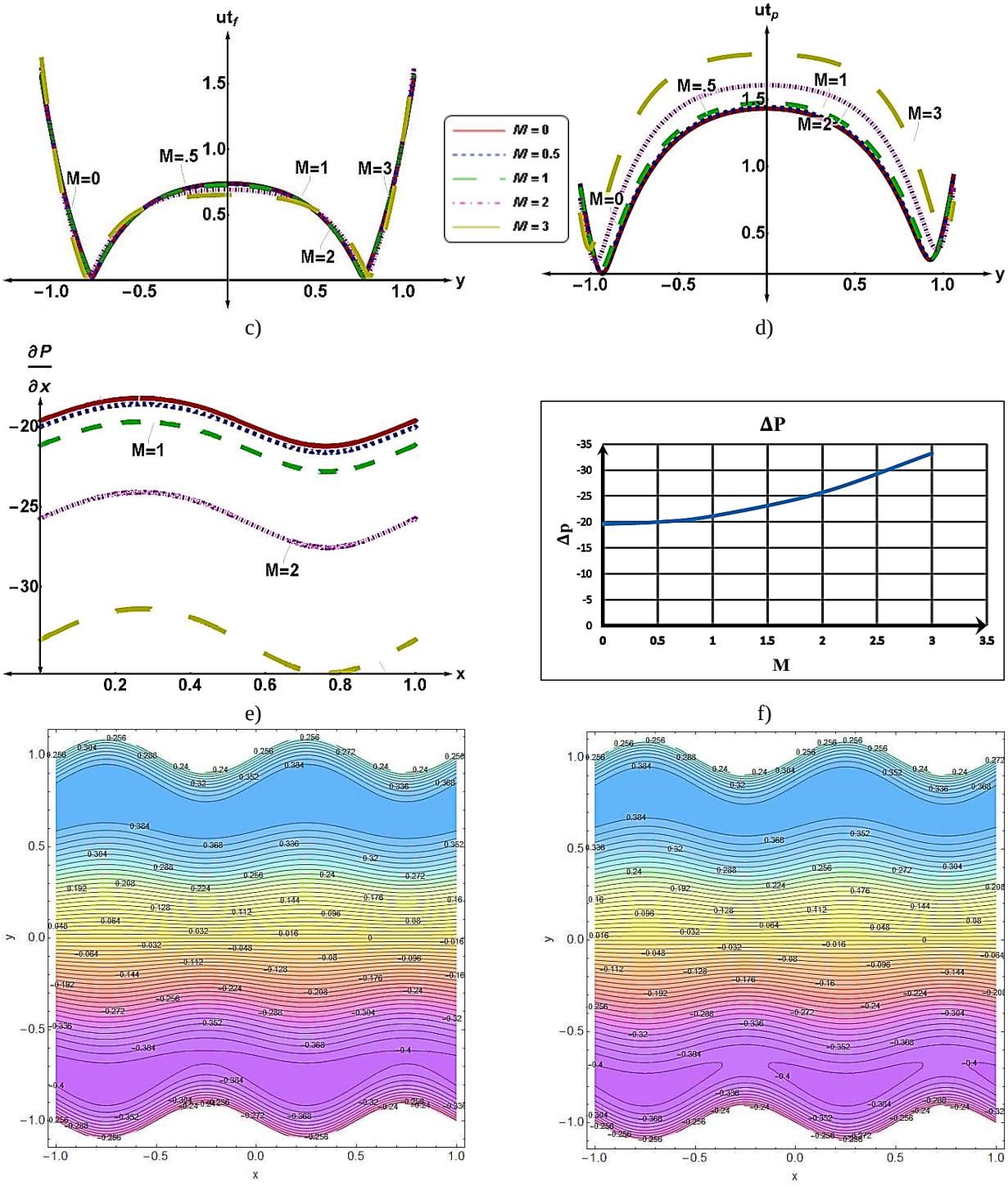

Figure 3 Influence of magnetic field on fluid and particles flow behavior

Figure 3 illustrates the impact of the magnetic field (M) on fluid and particle dynamics. Specifically, Figure 3a presents the fluid velocity profile at different magnetic field values. It is discernible that the presence of a magnetic field induces a reduction in the axial fluid velocity at the channel center. Conversely, Figure 3b, depicting the velocity profiles of particles, reveals an increase in the axial velocity of particles with a corresponding elevation in the magnetic parameter (M). Figures 3c and 3d elucidate the

influence of the magnetic field (M) on the total velocity of the fluid and particles, respectively. These figures demonstrate that the total velocity of the fluid diminishes while the total velocity of particles escalates with an augmentation of the magnetic parameter (M). Importantly, it is noteworthy that the normal velocity remains unaffected. The consequences of these velocity changes manifest in Figure 3e, where a reduction in fluid velocity corresponds to an increase in the pressure gradient. This phenomenon is further underscored in Figure 3f, wherein an elevation in the magnetic parameter (M) leads to an augmented pressure difference. Figures 3g and 3h depict the evolving streamlines as the magnetic field (M) intensifies. Notably, an emergent vortex near the lower wall becomes apparent with increasing magnetic field (M). This vortex exerts a constraining influence on the fluid, diminishing its velocity and consequently augmenting the pressure within the flow. Importantly, this rise in pressure contributes to an increase in the velocity of particles within the system.

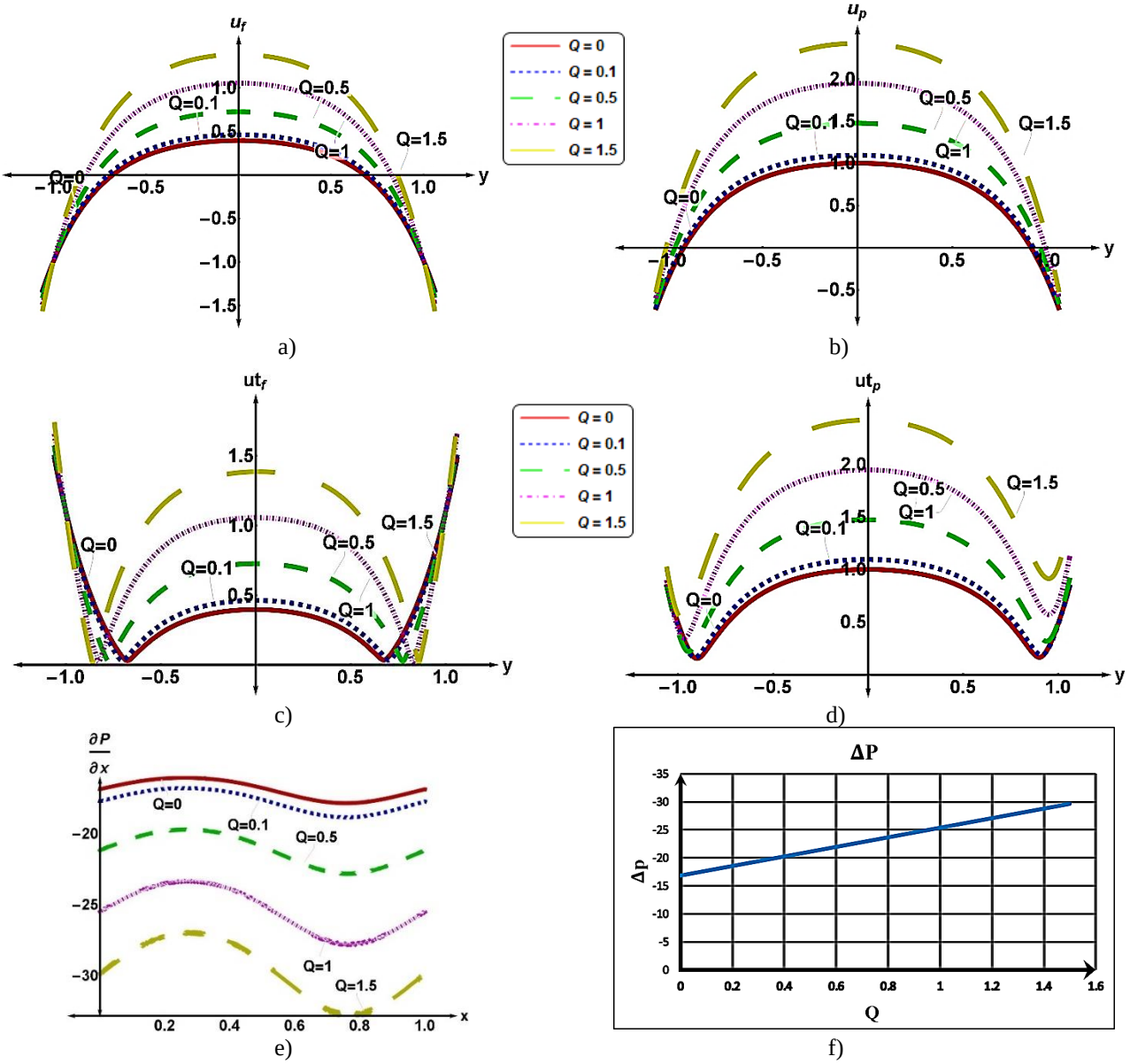

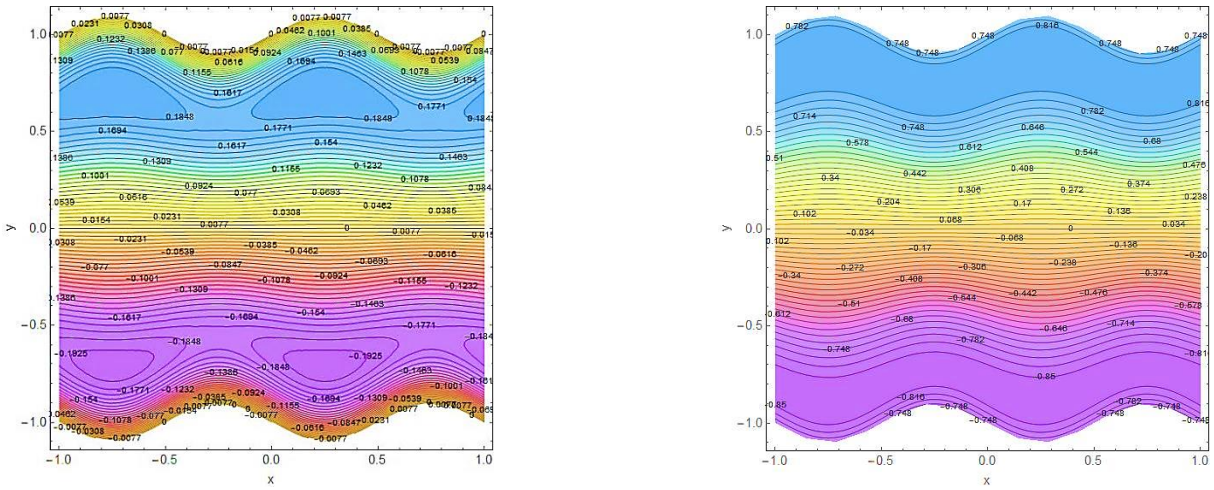

g) Q=0 h) Q=1

Figure 4 Effect of mean flow rate on fluid and particles flow behavior

The discernible impact of the mean flow rate (Q) on fluid and particle flow dynamics is elucidated in Figure 4. In Figure 4a, there is a conspicuous augmentation in the axial velocity of the fluid with the escalation of the flow rate (Q). This observed trend is parallel to a concurrent increase in fluid total velocity, as exemplified in Figure 4c. Such behavior can be ascribed to the amplification of the pressure gradient with the ascending mean flow rate (Q), as delineated in Figures 4e and 4f. Consequently, the particle velocity experiences a commensurate elevation, as elucidated in Figures 4b and 4d. Figures 4g and 4h provide nuanced insights into the repercussions of heightened flow rates on streamlines. Notably, an augmentation in flow rate (Q) manifests as a smoothing effect on the flow, evident through the evolving patterns illustrated in the streamlines. This observation is congruent with the overarching trend wherein increased flow rates contribute to a more cohesive and streamlined flow field.

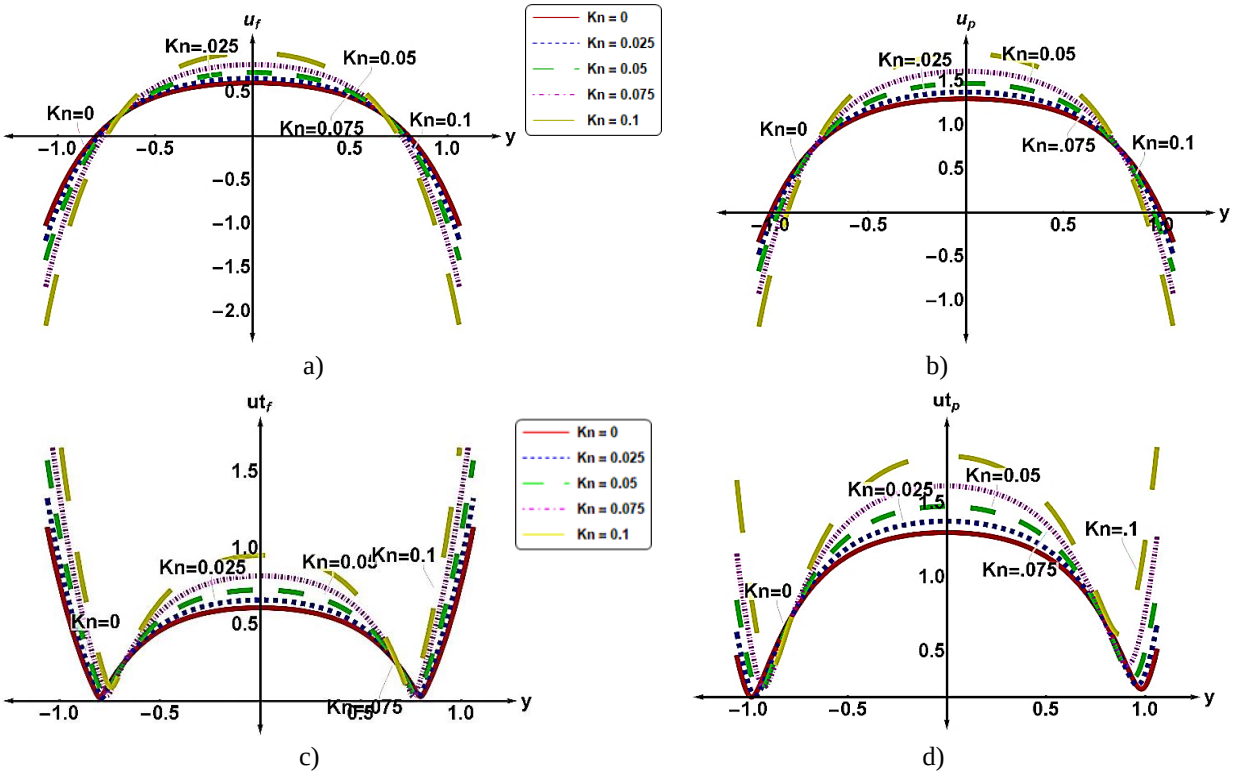

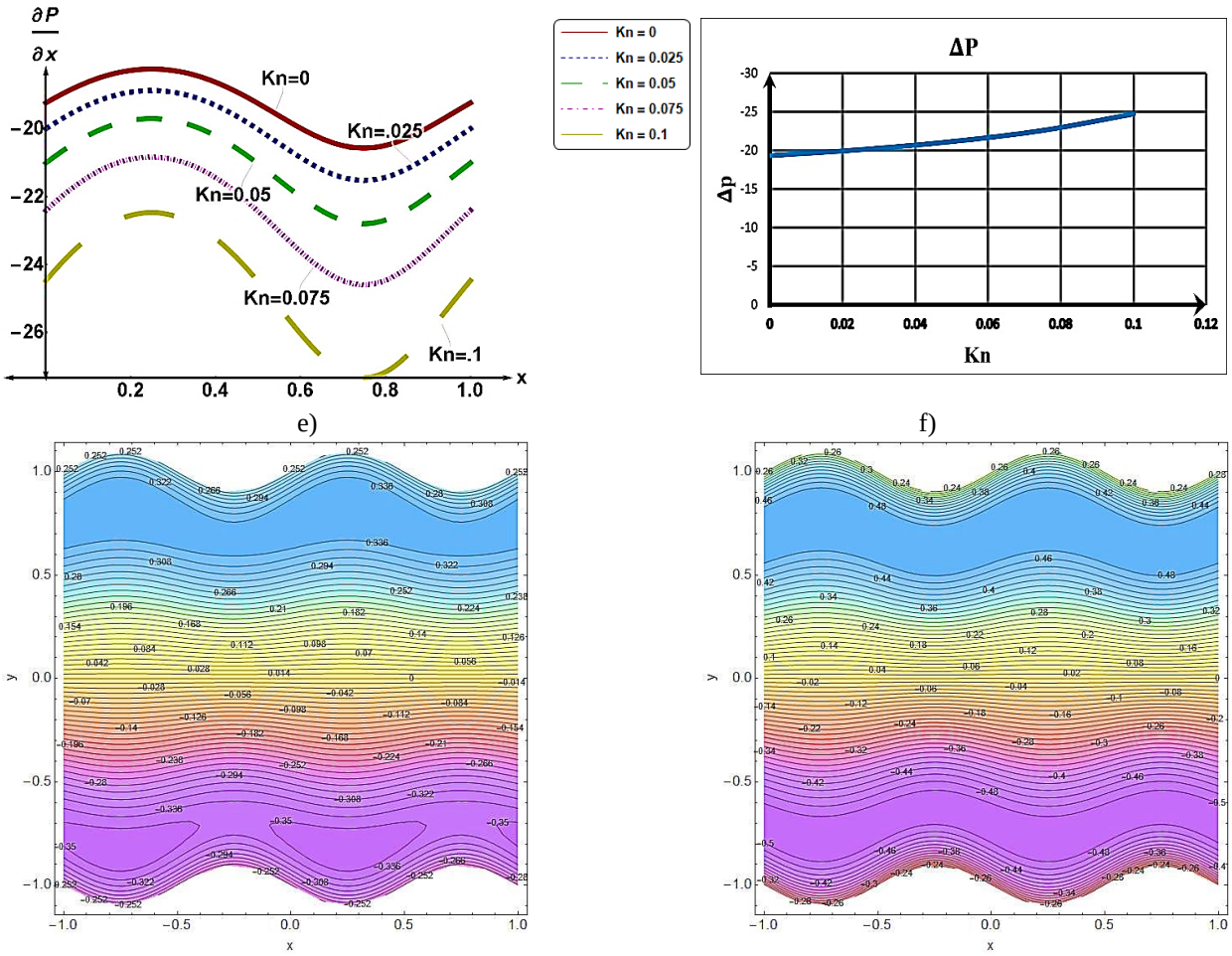

Figure 5 Effect of slipping (Kn) on fluid and particles flow behavior

Figure 5 illustrates the impact of slipping Knudsen number (Kn) on flow characteristics. The escalation of slip at the boundary results in an augmentation of fluid velocity at the boundary, consequently mitigating backflow effects at the boundaries. This leads to an acceleration of flow within the core zone of the channel, as depicted in Figure 5a. The influence of the slipping parameter (Kn) on the overall fluid velocity is depicted in Figure 5c, indicating an observed rise in velocity both at the channel's core and boundary regions. This is attributed to the heightened normal fluid velocity induced by slip conditions. Figures 5e and 5f present the pressure gradient and pressure difference at different (Kn) values. It is noted that increasing (Kn) induces an elevation in both pressure gradient and pressure difference. This phenomenon is attributable to the heightened fluid velocity at the boundaries resulting from increased slipping, intensifying the friction between the fluid and the wall surfaces. This heightened friction, in turn, leads to an augmentation in pressure differences. The consequential rise in pressure and fluid velocity contributes to an increase in axial and total particle velocity, as demonstrated in Figures 5b and 5d. The heightened Kn value correlates with an augmentation in total velocity at the channel's boundaries (Figure 5c), enhancing flow dynamics and diminishing vortex formation at the lower boundary induced by the presence of a magnetic field.

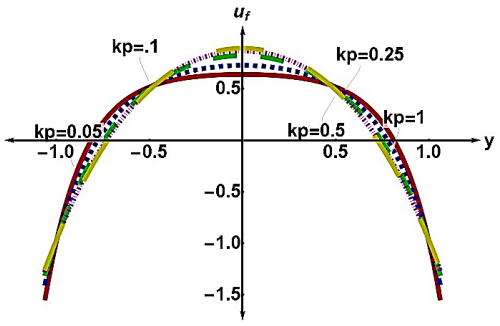

a)

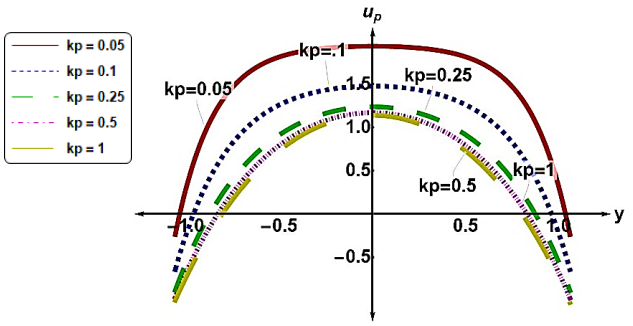

b)

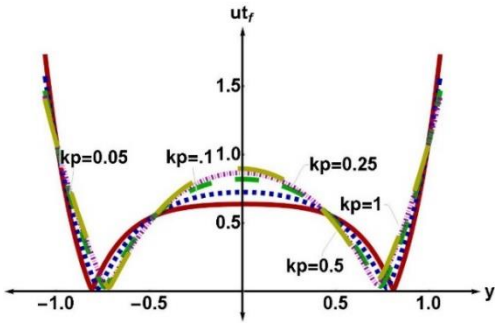

c)

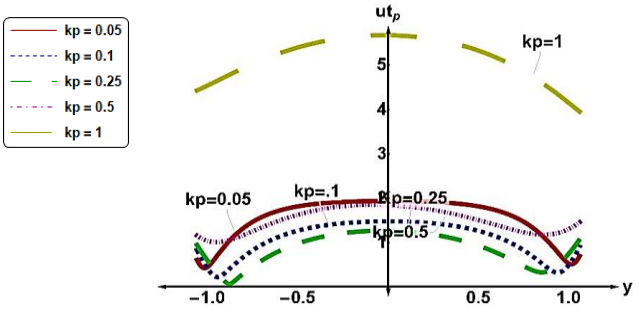

d)

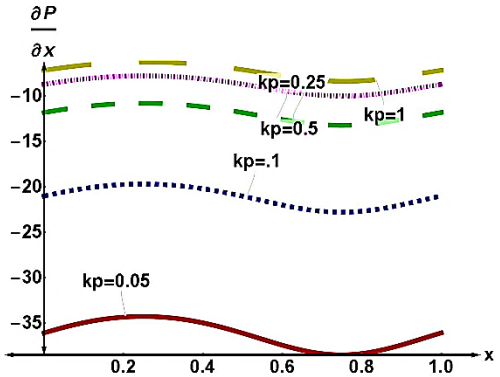

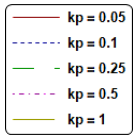

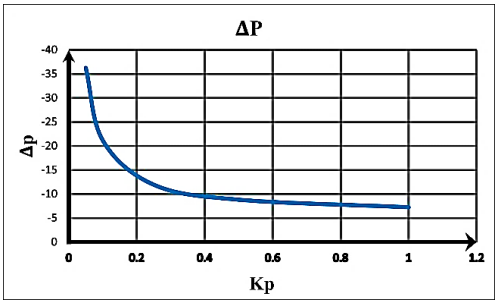

e) f)

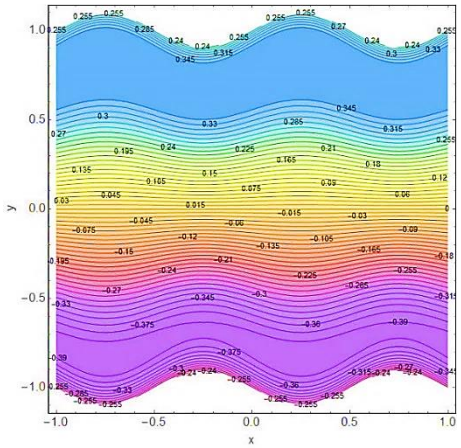

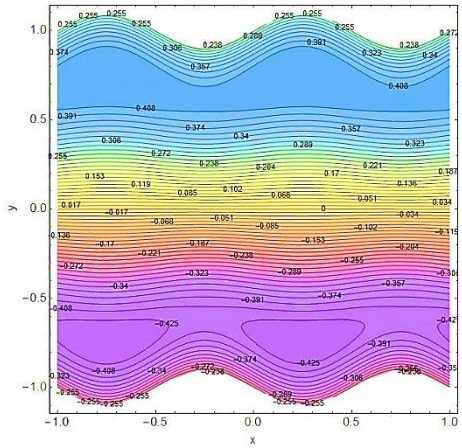

g) k_p=0.05 h) k_p =1

Figure 6 Effect of Permeability parameter (K_p) on fluid and particles flow

Figure 6 illustrates the impact of the permeability parameter (K_p) on the system. The permeability factor, denoted as (K_p,) characterizes the porous medium within a specified range ($0 \leq K_p \leq \infty$). A (K_p) value approaching infinity implies that 1/Kp equals zero, signifying an unimpeded pathway devoid of porosity. Conversely, when K_p equals zero, ($1/K_p$) tends toward infinity, indicating a pathway filled with spatial porosity, effectively obstructing the flow. Consequently, an elevation in (K_p) results in a reduction of porous medium presence. Observations from Figure 6a reveal that an increase in (K_p), which lead to increases the cross-section area of flowing the fluid leading to increases the axial fluid velocity in the center, with no discernible effect on the channel walls due to slipping existing. Simultaneously, fluid normal velocity experiences an increment, contributing to a notable rise in the total fluid velocity, as depicted in Figure 6c. Analysis of Figure 6b demonstrates that particle axial velocity exhibits an overall increase across the channel cross-section due to heightened fluid velocities. However, the total particle velocity experiences a reduction with increasing (K_p) until reaching (K_p=0.25), beyond which a subsequent rise in particle total velocity occurs (Figure 6d).The escalated velocities induce a decrease in pressure, evident in Figure 6e and 6f. Notably, the pronounced increase in fluid normal velocity results in the formation of vortices at the lower wall, attributed to the influence of the magnetic field, as illustrated in Figure 6g and 6h.

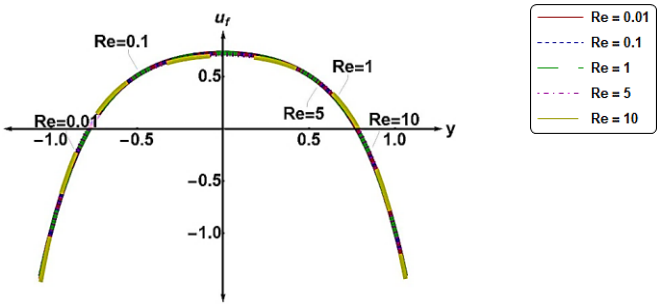

a)

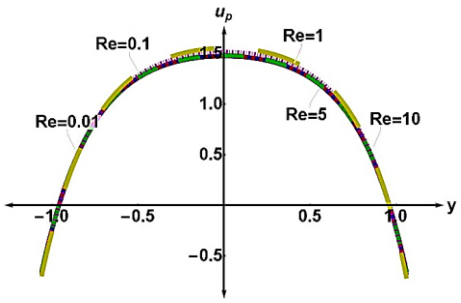

b)

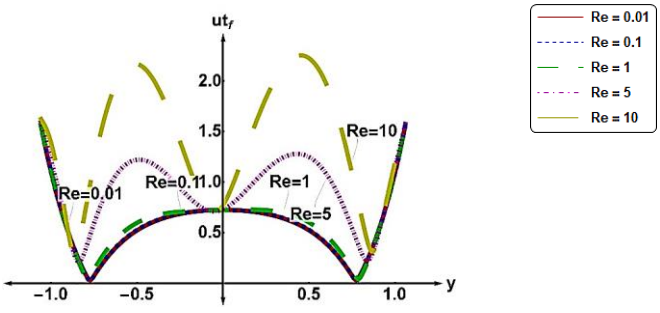

c)

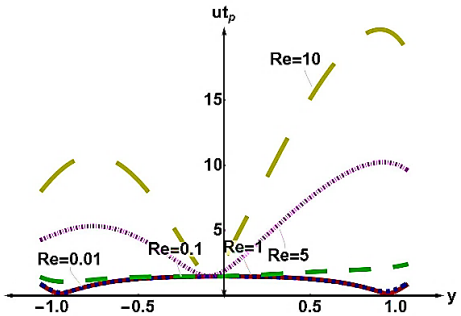

d)

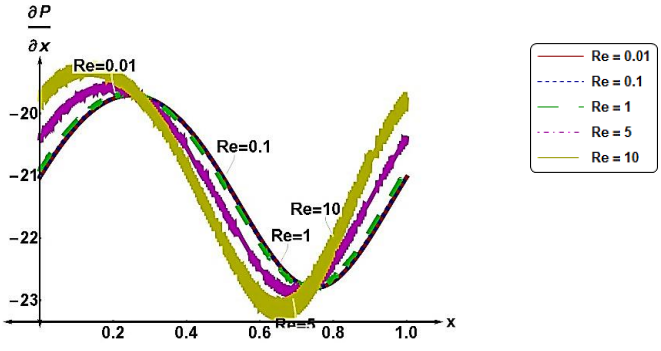

e)

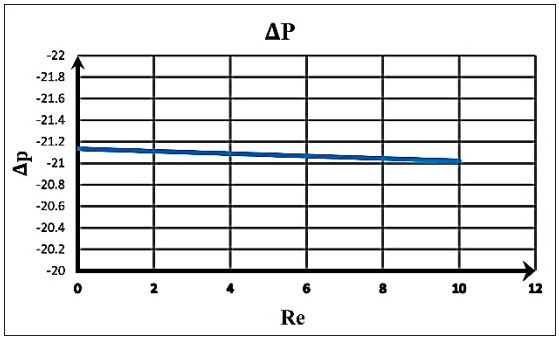

f)

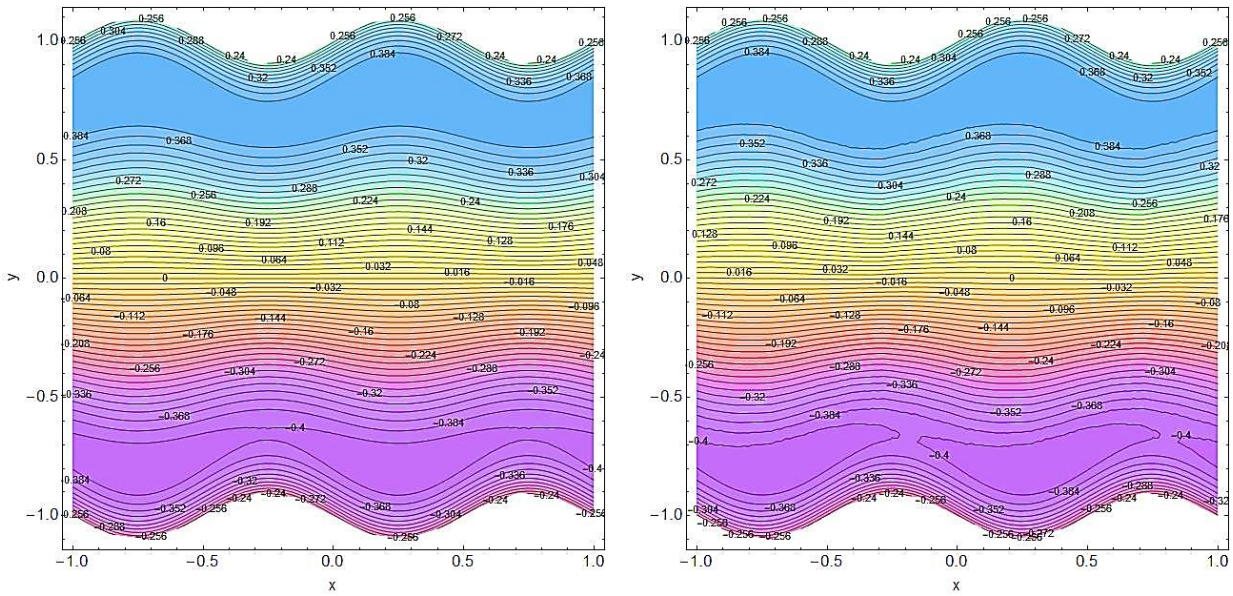

g) Re=0.01 h) Re=10

Figure7 Effect of Reynolds number (Re) on fluid and particles flow behavior

Figure 7 provides a comprehensive elucidation of the impact of Reynolds number (Re) on fluid dynamics. The Reynolds number, a dimensionless parameter crucial for characterizing fluid systems, plays a pivotal role in categorizing fluid behavior. An increase in Reynolds number results in an elevated inertia force within the mixture, consequently affecting the fluid through peristaltic motion along the channel walls. Figure 7a distinctly reveals that, as Reynolds number (Re) experiences an increment, the axial velocity of the fluid demonstrates a modest effect. Concurrently, the normal velocity of the fluid undergoes a rapid augmentation, primarily influenced by the presence of peristaltic motion of the walls. This phenomenon culminates in a conspicuous rise in the overall fluid velocity, as portrayed in Figure 7c. Notably, the escalation in particle axial velocity at the channel's center, depicted in Figure 7b, is attributed to the increasing fluid velocity. Simultaneously, the normal particle velocity undergoes a substantial surge, leading to a pronounced augmentation of the total particle velocity, as illustrated in Figure 7d. The observed escalation in velocity precipitates a reduction in the pressure gradient, as evidenced in Figure 7e. The introduction of wall roughness, in conjunction with an increasing Reynolds number (Re), induces discernible fluctuations in the pressure gradient. Particularly noteworthy is the substantial augmentation in fluid normal velocity, giving rise to vortex formation at the lower wall, attributable to the presence of a magnetic field, as exemplified in Figure 7g and 7h. This vortex formation contributes to a diminishing pressure difference with increasing Reynolds number (Re), as highlighted in Figure 7f.

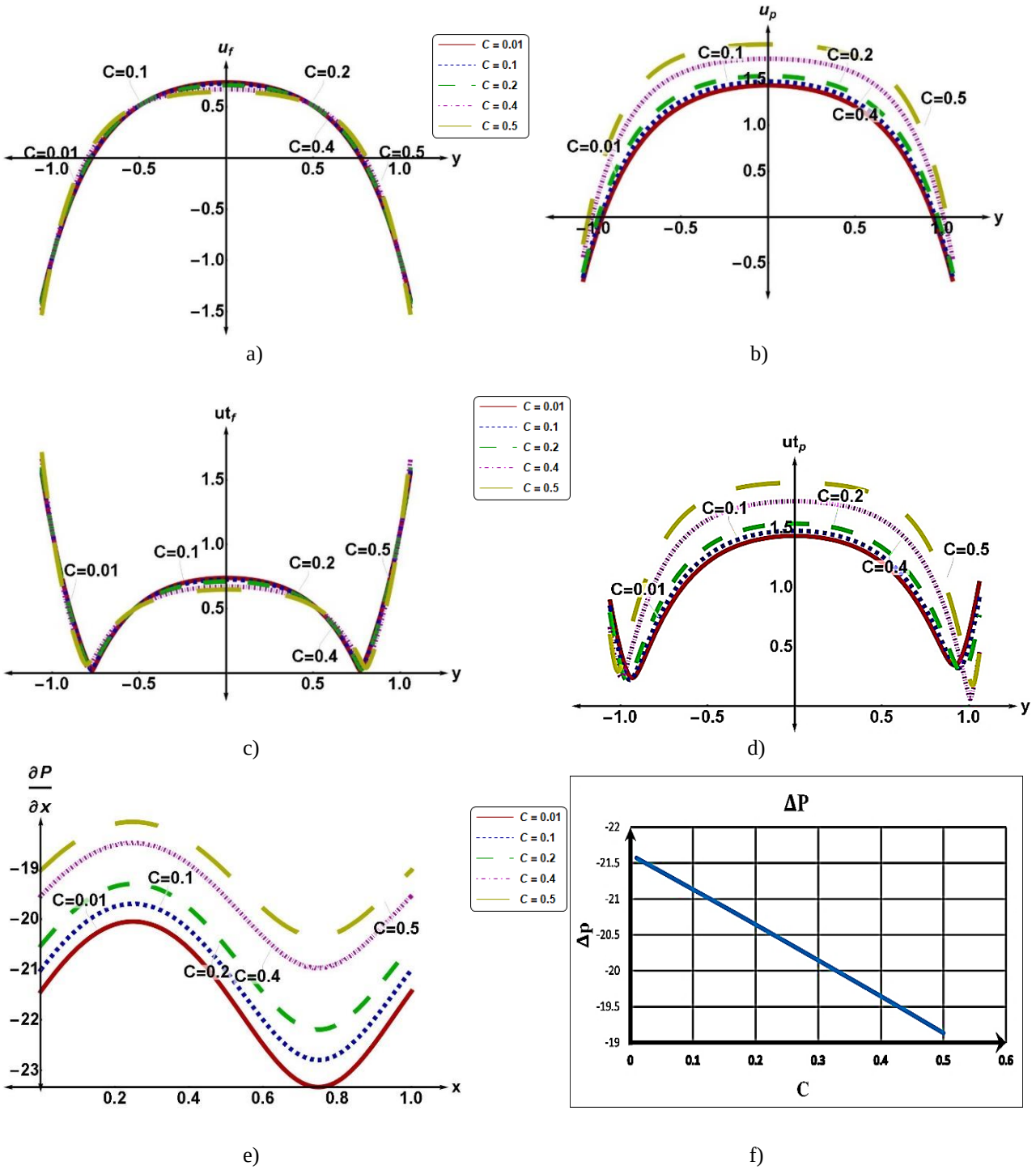

Figure 8 Effect of particle concentration (C) on fluid and particles flow behavior

Figure 8 provides insights into the impact of particle concentration (C) on the fluid dynamics. In the context of laminar flow, it becomes evident that an elevation in particle concentration (C) holds greater significance in influencing the channel's cross-sectional area compared to geometric size. This phenomenon results in a notable reduction in the cross-sectional area of the channel. This reduction, in turn, induces a decrease in fluid axial velocity at the core of the channel, as the flow is laminar , as elucidated in Figure

8a.Concomitantly, Figure 8b portrays an increase in the axial velocity of particles corresponding to the rise in particle concentration (C). This increase is attributed to the augmented area of particle exposure to pressure, leading to a subsequent enhancement in the total particle velocity, as depicted in Figure 8d.Moreover, an augmentation in particle concentration (C) manifests in a discernible reduction in fluid concentration, consequently causing a diminishment in the pressure gradient and pressure difference, as illustrated in Figures 8e and 8f, respectively

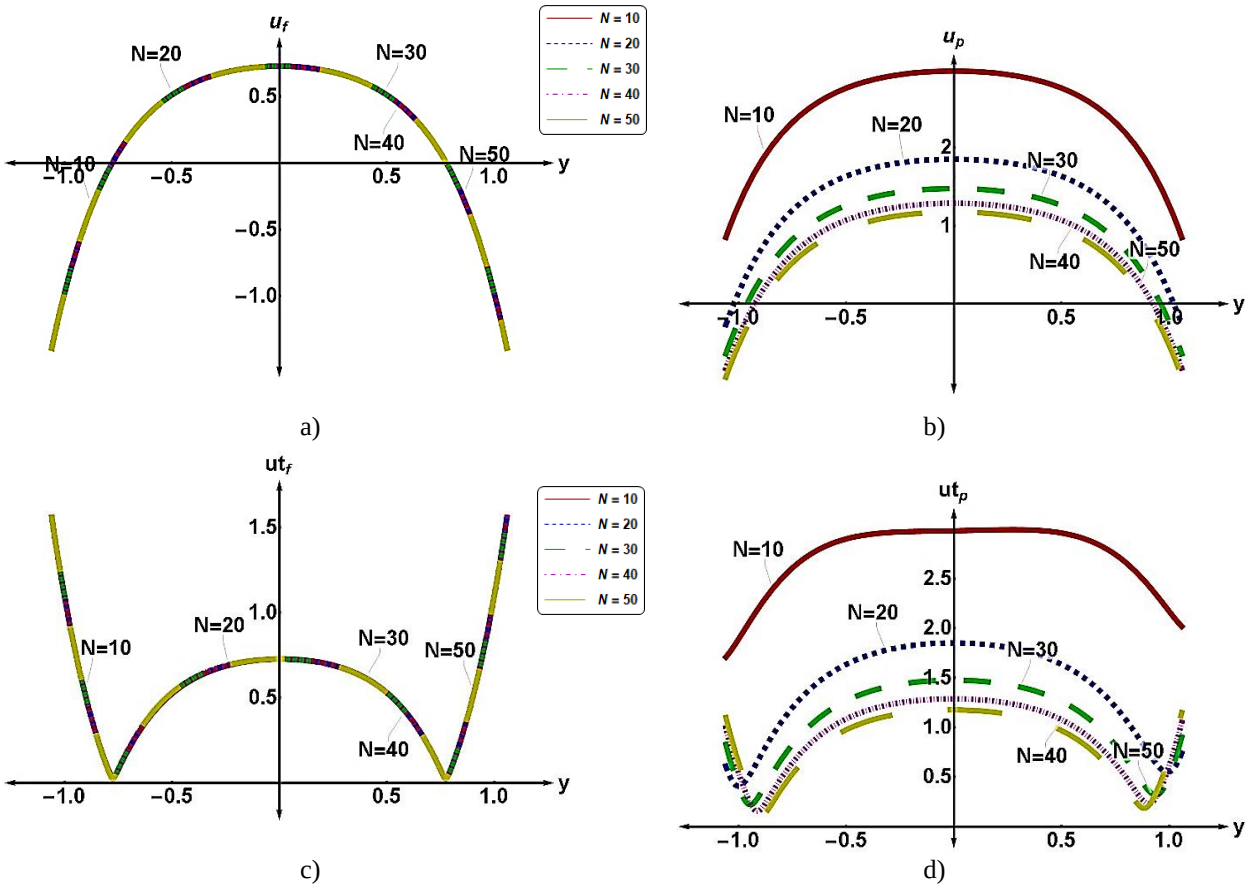

Figure 9 Effect of suspension factor (N) on fluid and particles flow behavior

The influence of the suspension factor (N) is elucidated in Figure 9, wherein a discernible positive correlation between the suspension factor (N) and the drag force exerted on the particle suspension is evident. Notably, an increase in the suspension factor (N) results in the effective axial velocity converging towards the fluid axial velocity, attributable to the mutual augmentation of forces between the fluid and particles, as illustrated in Figure 9b. Concurrently, the elevation of the suspension factor (N) precipitates a conspicuous decrement in the overall particle velocity, as depicted in Figure 9d. This observation underscores the substantial impact of the suspension factor (N) on the dynamic characteristics of particle-laden flows, particularly concerning the convergence of axial velocity and reduction in particle velocity. From a physical perspective, this phenomenon can be comprehended as the intensified interplay between the fluid and particulate components, leading to a more pronounced alignment of their velocities and consequential diminution in overall particle motion.

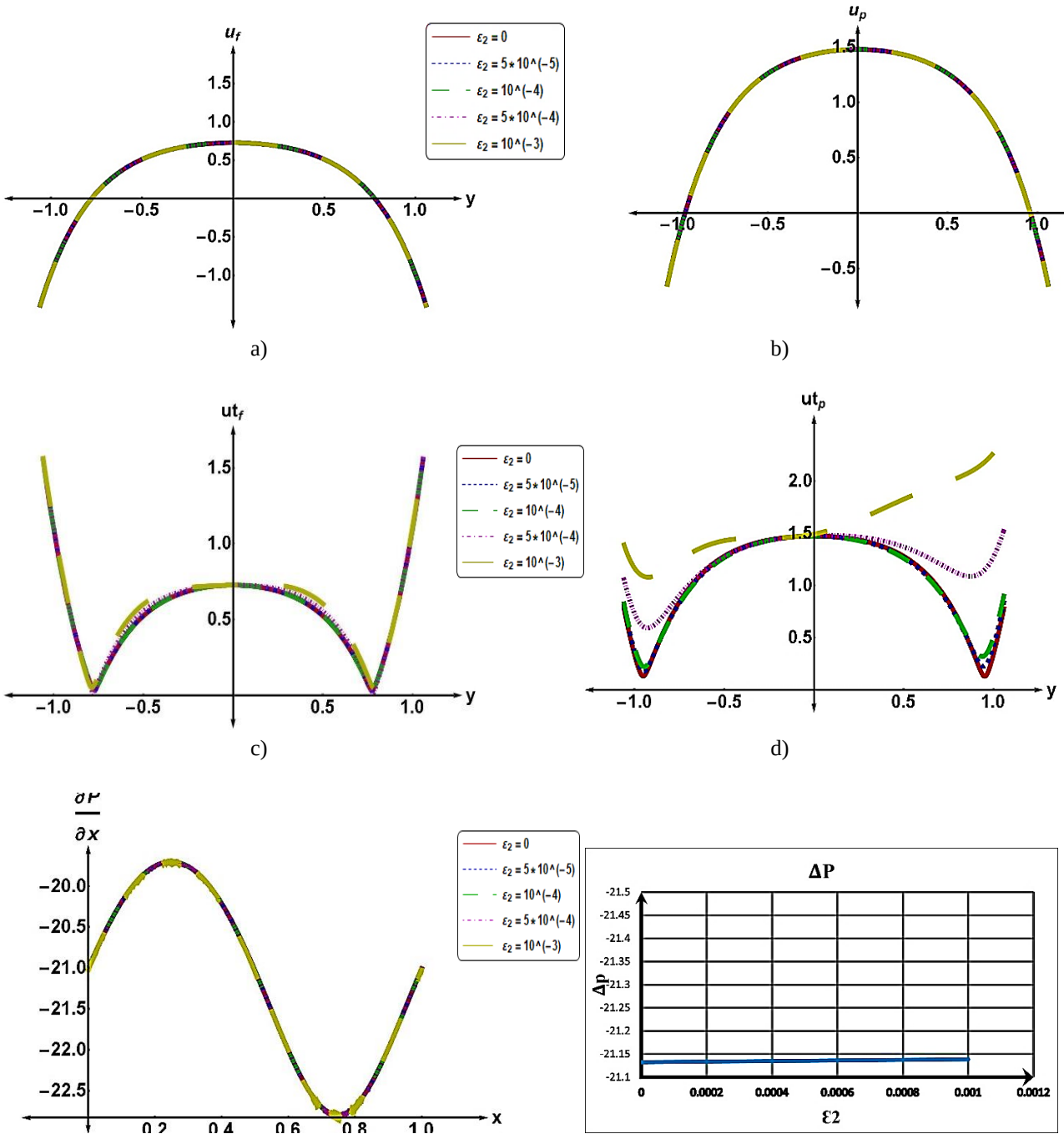

Figure10 Effect of wall roughness high ratio ($\boldsymbol{\varepsilon_2}$) on fluid and particles flow behavior

The impact of wall roughness characterized by the parameter (ε_2) is elucidated in Figure 10. Examination of Figure 10a and 10b reveals a marginal influence on both fluid and particle axial velocities with the progression of (ε_2), that due to the laminar fluid flow. However, Figure 10c illustrates a subtle enhancement

in fluid total velocity with increasing (ε_2). Notably, Figure 10d exhibits a noteworthy escalation in particle total velocity near the boundary, attributed to the augmentation of groove depth resulting from increased wall roughness (ε_2). This phenomenon induces fluctuations in the pressure gradient at the roughness site, as depicted in Figure 10e. Furthermore, the pressure difference, delineated in Figure 10f, demonstrates a gradual increment with rising values of (ε_2). The influence of wall roughness on the pressure differential is modest, given that the primary alterations in flow velocity manifest in the vertical component, exerting negligible impact on the axial velocity. This phenomenon stems from the laminar flow characteristics inherent in fluid dynamics, particularly within the domain of biofluids, which constitutes the primary subject of investigation in this study.

Table 1 Flow parameters

Parameter / Figure	M	Q	kn	K_p	Re	C	N	ε_2	Pr	λ	Gr	ρ_0	φ	β	ε_1	Nr
Figure 3	0 0.5 1 2 3	0.5	0.05	0.1	0.1	0.1	30	10^{-4}	1	0.005	0.9	5	0	1	0.1	1
Figure 4	1	0 0.1 0.5 1 1.5	0.05	0.1	0.1	0.1	30	10^{-4}	1	0.005	0.9	5	0	1	0.1	1
Figure 5	1	0.5	0 0.025 0.05 0.075 0.1	0.1	0.1	0.1	30	10^{-4}	1	0.005	0.9	5	0	1	0.1	1
Figure 6	1	0.5	0.05	0.05 0.1 0.25 0.5 1	0.1	0.1	30	10^{-4}	1	0.005	0.9	5	0	1	0.1	1
Figure 7	1	0.5	0.05	0.1	0.01 0.1 1 5 10	0.1	30	10^{-4}	1	0.005	0.9	5	0	1	0.1	1
Figure 8	1	0.5	0.05	0.1	0.1	0.01 0.1 0.2 0.4 0.5	30	10^{-4}	1	0.005	0.9	5	0	1	0.1	1
Figure 9	1	0.5	0.05	0.1	0.1	0.1	10 20 30 40 50	10^{-4}	1	0.005	0.9	5	0	1	0.1	1
Figure 10	1	0.5	0.05	0.1	0.1	0.1	30	0 $5x10^{-5}$ $1x10^{-4}$ $5x10^{-4}$ $1x10^{-4}$	1	0.005	0.9	5	0	1	0.1	1

Conclusions

This study systematically examines the collective influences of the magnetic field (M), volumetric flow rate (Q), slip parameter (Kn), space porosity (K_p), solid suspensions (C), and particle factors on the dynamics of fluid and particle flow within a wall roughness channel under the influence of peristaltic transport. Employing the analytical perturbation technique, we rigorously solve the governing equations through a specific procedural approach, yielding mathematical expressions for both fluid and particle streamlines. The derived axial and total velocity profiles for fluid and particle flow, as well as the pressure gradient and pressure difference, are presented.

Key findings from our investigation include:

- Enhancement of the magnetic field (M) results in a reduction of fluid velocity, consequently elevating pressure and inducing an increase in particle velocity.
- An escalation in the mean flow rate (Q) corresponds to an increased flow pressure, leading to heightened fluid and particle velocities.
- The introduction of slipping (Kn) amplifies both fluid and particle velocities while mitigating the impact of vortices generated by the magnetic field near the lower channel wall.
- The incorporation of a porous medium diminishes fluid velocity, consequently augmenting pressure within the system.
- Increased Reynolds numbers contribute to elevated fluid and particle axial velocities near the wall, fostering vortex formation at the lower wall.
- The suspension factor exclusively influences particle velocity, with an escalation in (N) causing the particle velocity to approach the fluid velocity at the channel core.
- Wall roughness height ratio (ε_2) significantly impacts axial velocity, primarily through the increase in wall roughness height.

The principal aim of this investigation is to attain a nuanced understanding of fluid dynamics, with a particular focus on the peristaltic flow of essential fluids, including blood and its constituents, within the human circulatory system. Moreover, the ramifications of these findings have broad-reaching implications across both biological and industrial domains, encompassing applications in magnetic resonance imaging (MRI) and radiosurgery.

References

[1] T. W. Latham, "Fluid Motion in a Peristaltic Pump," MSc thesis, Massachusetts Institute of Technology, Cambridge, MA, 1966.

[2] M. Y. Jaffrin and A. H. Shapiro, "Peristaltic pumping," Annu Rev Fluid Mech, vol. 3, pp. 13-16, 1971.

[3] C. Barton and S. Raynor, "Bull. Math. Biophys. 30, 663-680," 1968.

[4] T. Fung and C. Yih, "Peristaltic transport," Trans ASME J Appl Mech, vol. 35, pp. 669-675, 1968.

[5] M. Mishra and A. R. Rao, "Peristaltic transport of a Newtonian fluid in an asymmetric channel," Z Angew Math Phys, vol. 54, pp. 532-550, 2003

[6] T. S. Tenforde, "Magnetically induced electric fields and currents in the circulatory system," Prog Biophys Mol Biol, vol. 87, pp. 279, 2008.

[7] V. E. R. T. Mooney, "A randomized double-blind prospective study of the efficacy of pulsed electromagnetic fields for interbody lumbar fusions," Spine, vol. 15, no. 7, pp. 708-712, 1990.

[8] V. K. Sud, G. S. Sekhon, and R. K. Mishra, "Pumping action on blood by a magnetic field," Bulletin of mathematical biology, vol. 39, no. 3, pp. 385-390, 1977.

[9] H. L. Agrawal and B. Anwaruddin, "Peristaltic flow of blood in a branch," Ranchi Univ. Math. J, vol. 15, pp. 111-121, 1984.

[10] K. S. Mekheimer, "Peristaltic flow of blood under effect of a magnetic field in non-uniform channels," Applied Mathematics and Computation, vol. 153, no. 3, pp. 763-777, 2004.

[11] N. Mustapha, N. Amin, S. Chakravarty, and P. K. Mandal, "Unsteady magnetohydrodynamic blood flow through irregular multi-stenosed arteries," Computers in Biology and Medicine, vol. 39, no. 10, pp. 896-906, 2009.

[12] E. E. Tzirtzilakis and V. C. Loukopoulos, "Biofluid flow in a channel under the action of a uniform localized magnetic field," Comput Mech, vol. 36, pp. 360-374, 2005

[13] E. E. Tzirtzilakis and M. Xenos, "Biomagnetic fluid flow in a driven cavity," Meccanica, vol. 48, pp. 187-200, 2013.

[14] B. K. Sharma, M. Sharma, R. K. Gaur, and A. Mishra, "Mathematical modeling of magneto pulsatile blood flow through a porous medium with a heat source," International Journal of Applied Mechanics and Engineering, vol. 20, no. 2, pp. 385-396, 2015.

[15] E. F. El-Shehawey and W. El-Sebaei, "Couple-stress in peristaltic transport of a magneto-fluid," Physica Scripta, vol. 64, no. 5, pp. 401, 2001.

[16] T. Hayat et al., "Peristaltic flow of a second-order fluid in the presence of an induced magnetic field," International journal for numerical methods in fluids, vol. 67, no. 5, pp. 537-558, 2011.

[17] M. Rashid, K. Ansar, and S. Nadeem, "Effects of induced magnetic field for peristaltic flow of Williamson fluid in a curved channel," Physica A, vol. 2020, pp. 1-29, https://doi.org/10.1016/j.physa.2019.123979

[18] R. M. Abumandour, I. M. Eldesoky, and E. T. Abdelwahab, "On the Performance of Peristaltic Pumping for the MHD Slip Flow under the Variation of Elastic Walls Features," ERJ. Engineering Research Journal, vol. 43, no. 3, pp. 231-244, 2020

[19] G. Radhakrishnamacharya and V. Radhakrishna Murty, "Heat Transfer to Peristaltic in a Non-Uniform Channel," Defence Science Journal, vol. 43, no. 3, pp. 275, 1993.

[20] S. Srinivas and M. Kothandapani, "Peristaltic transport in an asymmetric channel with heat transfer—a note," International Communications in Heat and Mass Transfer, vol. 35, no. 4, pp. 514-522, 2008.

[21] S. Nadeem and N. S. Akbar, "Effects of heat transfer on the peristaltic transport of MHD Newtonian fluid with variable viscosity: application of Adomian decomposition method," Commun Nonlin Sci Numer Simul, vol. 14, pp. 3844-3855, 2009.

[22] S. R. Mishra, G. C. Dash, and M. Acharya, "Mass and heat transfer effect on MHD flow of a visco-elastic fluid through porous medium with oscillatory suction and heat source," International Journal of Heat and Mass Transfer, vol. 57, no. 2, pp. 433-438, 2013.

[23] A. Mahmood, M. F. Md Basir, U. Ali, M. S. Mohd Kasihmuddin, and M. A. Mansor, "Numerical Solutions of Heat Transfer for Magnetohydrodynamic Jeffery-Hamel Flow Using Spectral Homotopy Analysis Method," Processes, vol. 7, no. 9, pp. 626, 2019.

[24] T. Hayat, M. U. Qureshi, and Q. Hussain, "Effect of heat transfer on the peristaltic flow of an electrically conducting fluid in a porous space," Applied Mathematical Modelling, vol. 33, no. 4, pp. 1862-1873, 2009.

[25] Q. M. Ali, Z. Farooq, U., D. Lu, "Investigation of Entropy in Two-Dimensional Peristaltic Flow with Temperature-Dependent Viscosity, Thermal, and Electrical Conductivity," Entropy, vol. 22, no. 2, p. 200, 2020.

[26] E. F. El Shehawey, et al., "Peristaltic transport through a porous medium," J. Biomath, vol. 14, no. 1, pp. 1-13, 1999.

[27] E. F. El-Shehawey and W. El Sebaei, "Peristaltic transport in a cylindrical tube through a porous medium," International Journal of Mathematics and Mathematical Sciences, vol. 24, no. 4, pp. 217-230, 2000.

[28] E. F. Elshehawey, N. T. Eldabe, E. M. Elghazy, and A. Ebaid, "Peristaltic transport in an asymmetric channel through a porous medium," *Appl. Math. Comput.*, vol. 182, no. 1, pp. 140-150, 2006..

[29] T. Hayat, M. Javed, and N. Ali, "MHD peristaltic transport of a Jeffery fluid in a channel with compliant walls and porous space," Transport in Porous Media, vol. 74, no. 3, pp. 259-274, 2008.

[30] J. C. Umavathi, I. C. Liu, and J. Prathap-Kumar, "Unsteady flow and heat transfer of porous media sandwiched between viscous fluids," Appl. Math. Mech., vol. 31, no. 12, pp. 1497-1516, 2010.

[31] W. Chu and J. Fang, "Peristaltic transport in a slip flow," The European Physical Journal B-Condensed Matter and Complex Systems, vol. 16, no. 3, pp. 543-547, 2000.

[32] N. Ali, Q. Hussain, T. Hayat, and S. Asghar, "Slip effects on the peristaltic transport of MHD fluid with variable viscosity," Phys. Lett. A vol. 372, no. 8, pp. 1477–1489, 2008.

[33] A. Sinha, G. Shit, and N. Ranjit, "Peristaltic transport of MHD flow and heat transfer in an asymmetric channel: effects of variable viscosity, velocity-slip, and temperature jump," Alex. Eng. J., vol. 54, no. 3, pp. 691–704, 2015.

[34] K. Vajravelu, S. Sreenadh R. Saravana, "Combined influence of velocity slip, temperature, and concentration jump conditions on MHD peristaltic transport of a Carreau fluid in a non-uniform channel," Appl. Math. Comput., vol. 225, pp. 656–676, 2013.

[35] I. Eldesoky, S. I. Abdelsalam, W. A. El-Askary, and M. Ahmed, "The integrated thermal effect in conjunction with slip conditions on peristaltically induced particle-fluid transport in a catheterized pipe," Journal of Porous Media, vol. 23, no. 7, 2020

[36] T.-K. Hung and T. D. Brown, "Solid-particle motion in two-dimensional peristaltic flows," J. Fluid Mech., vol. 73, no. 1, pp. 77-96, 1976.

[37] H. Rath and G. Reese, "Peristaltic flow of non-Newtonian fluids containing small spherical particles," Arch. Mech., vol. 36, no. 2, pp. 263-277, 1984.

[38] V. P. Srivastava and L. M. Srivastava, "Effects of Poiseuille flow on peristaltic transport of a particulate suspension," ZAMP, vol. 46, no. 5, pp. 655-679, 1995.

[39] Kh. S. Mekheimer, E. F. El Shehawey, and A. M. Elaw, "Peristaltic motion of a particle-fluid suspension in a planar channel," Int. J. Theor. Phys., vol. 37, no. 11, pp. 2895-2920, 1998.

[40] S. I. Abdelsalam and K. Vafai, "Particulate suspension effect on peristaltically induced unsteady pulsatile flow in a narrow artery: blood flow model," Mathematical Biosciences, vol. 283, pp. 91-105, 2017.

[41] I. M. Eldesoky et al., "Interaction between compressibility and particulate suspension on peristaltically driven flow in planar channel," Applied Mathematics and Mechanics, vol. 38, no. 1, pp. 137-154, 2017.

[42] I. M. Eldesoky et al., "Concurrent Development of Thermal Energy with Magnetic Field on a Particle-Fluid Suspension Through a Porous Conduit," BioNanoScience, vol. 9, no. 1, pp. 186-202, 2019.

[43] M. M. Bhatti, A. Zeeshan, and R. Ellahi, "Study of heat transfer with nonlinear thermal radiation on sinusoidal motion of magnetic solid particles in a dusty fluid," Journal of Theoretical and Applied Mechanics, vol. 46, no. 3, pp. 75, 2016.

[44] M. H. Kamel, I. M. Eldesoky, B. M. Maher, and R. M. Abumandour, "Slip effects on peristaltic transport of a particle-fluid suspension in a planar channel," Applied bionics and biomechanics, vol. 2015, 2015.

[45] S. W. Park, M. Intaglietta, and D. M. Tartakovsky, "Impact of Endothelium Roughness on Blood Flow," Journal of Theoretical Biology, vol. 300, pp. 152-160, 2012.

[46] R. Shukla, S. S. Bhatt, A. Medhavi, and R. Kumar, "Effect of Surface Roughness during Peristaltic Movement in a Nonuniform Channel," Mathematical Problems in Engineering, vol. 2020.

[47] R. Shukla \textit{et al.}, "Mathematical analysis of heat transfer in peristaltic transport through a rough nonuniform inclined channel," \textit {Mathematical Problems in Engineering}, 2020.

[48] A. H. Nayfeh, "Perturbation Methods," John Wiley & Sons, 2008.

[49] Eldesoky, I. M., R. M. Abumandour, M. H. Kamel, and E. T. Abdelwahab. "The combined effects of wall properties and space porosity on MHD two-phase peristaltic slip transport through planar channels." International Journal of Applied and Computational Mathematics 7 (2021): 1-37.

[50] S. I. Abdelsalam, A. Magesh, P. Tamizharasi, and A. Zaher, "Versatile response of a Sutterby nanofluid under activation energy: hyperthermia therapy," International Journal of Numerical Methods for Heat & Fluid Flow, 2023.

[51] S. I. Abdelsalam, A. M. Alsharif, Y. Abd Elmaboud, and A. Abdellateef, "Assorted kerosene- based nanofluid across a dual-zone vertical annulus with electroosmosis," Heliyon, vol. 9, no. 5, 202